UNIVERSITÉ DE MONTRÉAL

TOWARDS RADIO ANALOG SIGNAL PROCESSING

BABAK NIKFAL
DÉPARTEMENT DE GÉNIE ÉLECTRIQUE
ÉCOLE POLYTECHNIQUE DE MONTRÉAL

THÈSE PRÉSENTÉE EN VUE DE L'OBTENTION
DU DIPLÔME DE PHILOSOPHIÆ DOCTOR
(GÉNIE ÉLECTRIQUE)
FÉVRIER 2015

UNIVERSITÉ DE MONTRÉAL

ÉCOLE POLYTECHNIQUE DE MONTRÉAL

Cette thèse intitulée:

TOWARDS RADIO ANALOG SIGNAL PROCESSING

présentée par: NIKFAL Babak
en vue de l'obtention du diplôme de: Philosophiæ Doctor
a été dûment acceptée par le jury d'examen constitué de:

M. AKYEL Cevdet, Ph. D., président
M. CALOZ Christophe, Ph. D., membre et directeur de recherche
M. DESLANDES Dominic, Ph. D., membre
M. KOUKI Ammar, Ph. D., membre externe

DEDICATION

To my family . . .

ACKNOWLEDGMENTS

I would like to thank my supervisor, Prof. Christophe Caloz, for his inspiring guidance, advice and support throughout this work.

I would like to thank my colleagues of the Caloz's Research Group for their help and collaborations. A special thank to Dr. Shulabh Gupta, my friend and colleague, for his excellent ideas and help during my research life. Thanks to Dimitrios, Nima, Sajjad, Qingfeng, Lianfeng, Karim, Zoé, Mohamed, Burak, Louis-Phillipe, Amar, Mario for their time and guidance in the group. Thanks also to Pascal, Lydia, Ajay, Farshad, Shabnam, Tahereh, Ramin, Amirhossein, Nasser, Faezeh, Hadi, Masood, and other people in Poly-Grames whom I bothered during past few years and shared happy times with me.

I would like to acknowledge the members of my thesis jury, Prof. Cevdet Akyel, Prof. Ammar Kouki and Prof. Dominic Deslandes, for having accepted to examine this work and for their valuable comments.

Also a special thank goes to Prof. Ke Wu, director of Poly-Grames Research Center of École Polytechnique de Montréal for all his kind support and encouragement.

I would like to acknowledge all technical staffs of Poly-Grames Research Center, Mr. Jules Gauthier, Mr. Traian Antonescu, Mr. Steve Dubé, Mr. Maxime Thibault, and Mr. Jean-Sebastien Décarie for assisting me in the fabrication and realization of my designs.

RÉSUMÉ

La demande insatiable pour les services de radio et communication à large bande, stimule les fabricants à chercher des nouvelles façons d'augmenter la largeur de bande spectrale des systèmes. Traitement numérique du signal (DSP) comme la technologie la plus commune des radios d'aujourd'hui est souple, reproductible, compact, et fiable à basse fréquence. Cependant, le système digital est plage dynamique limitée, le largeur de bande du système DSP est limité par la fréquence d'échantillonnage. À haute fréquence, telles que la fréquence d'onde millimétrique, le système DSP a un manque de performance et une consommation de puissance excessive. En outre, la complexité et le coût de système augmente aux fréquences plus élevées. Contrairement à DSP, les systèmes traitement radio-analogique du signal (R-ASP) sont bonnes performances à haute fréquence. Les systèmes R-ASP manipulent des signaux à large bande, temporellement sous leur forme analogique d'origine. Donc, ils n'ont pas besoin des convertisseurs A/D et D/A, et des convertisseurs haut/bas, résultant complexité inférieure à vitesse plus élevée, ce qui peut offrir des solutions sans précédent dans le domaine de l'ingénierie de radio. Phaser comme une structure de délai dispersive (DDS) contrôlable est le noyau d'un système R-ASP. Les composantes des fréquences du signal dans le temps se différencient après avoir traversé un phaser. Cette caractéristique du phaser le rend pratique pour l'application radio analogique haute vitesse, comme renifleur de spectre, multiplexage par division de fréquence (FDM), et impulsion radio.

Cette thèse par articles présente les concepts et les améliorations R-ASP en base de phaser, comme une alternative potentielle au traitement basé sur DSP, pour l'application de radio haute fréquence et haute vitesse. Le premier Chapitre traite de la motivation R-ASP, contributions de la thèse et de l'organisation. Les concepts et les caractéristiques du phaser, les nouvelles techniques pour améliorer la dispersion des phasers ainsi que la performance du système R-ASP, en fonction des applications sont proposées dans le Chapitre 2. Les Chapitres 3 à 6 sont les articles qui introduisent des nouvelles applications du R-ASP. Dans le Chapitre 3, une nouvelle technique de loop afin d'améliorer la résolution du phaser est proposé. En plus des fréquence mètres et les discriminateurs de fréquence, cette technique peut facilement appliquer à divers autres systèmes en temps réel, tels que les transformateurs de Fourier en temps réel, convolveurs, corrélateurs, et les radars compressifs. Le système Radio-ASP comporte un grand nombre d'applications dans le régime d'impulsion. Cependant, la génération d'impulsion UWB est complexe et coût élevé. Cette question est abordée dans le Chapitre 4, en proposant une technique de compression d'impulsion à faible coût pour la génération d'impulsions UWB. Dans le Chapitre 5, un phaser avec un retard de groupe etapé (stepped

group delay phaser) est proposé pour l'application de reniflement de spectre en temps réel. Le système écoute son environnement radio par une antenne, et détermine la présence ou l'absence des canaux actifs dans cet environnement. Le renifleur de spectre peut trouver son application dans les systèmes de radiocommunication cognitif. Dans le Chapitre 6, le concept d'amélioration de SNR pour l'impulsion radio à l'aide du phaser est démontré expérimentalement. Ici, la mise en valeur de SNR de l'impulsion radio est réalisé pour le bruit impulsif, bruit Gaussien et les brouilleurs à basse vitesse. Enfin, les conclusions et les travaux futurs du R-ASP sont présentés dans le Chapitre 8.

ABSTRACT

Insatiable demand for broadband radio and communication services spurs the manufacturers to seek new ways to increase the spectral bandwidth of the systems. Digital Signal Processing (DSP) as the most common technology of Today's radios is flexible, reproducible, compact, and reliable at low spectral bandwidth. However, digital system is limited precision and dynamic range. The bandwidth of the DSP system is limited by sampling rate. At high frequency, such as millimeter-wave frequency, the DSP system is poor performance and power hungry. Moreover, the complexity and cost of the system increase at higher frequency. In contrast of DSP, Radio-Analog Signal Processing (R-ASP) systems have a good performance at high frequency. R-ASP systems manipulate broadband signals, temporally in their original analog form. So, They don't need A/D and D/A, and up/down converters, resulting lower complexity at higher speed, which may offer unprecedented solutions in the major areas of radio engineering. Phaser as an engineerable dispersive delay structure (DDS) is the core of an R-ASP system. The component frequencies of the signal differentiate in time after passing through a phaser. This characteristic of the phaser makes it convenient for high speed analog radio application, such as frequency sniffer, frequency division multiplexing (FDM), and impulse radio.

This paper based dissertation introduces R-ASP concepts and enhancements, based on the phaser, as a potential alternative to DSP-based processing, for high speed and high frequency radio applications. The first Chapter discusses R-ASP motivation, thesis contributions and organization. The concepts of the phaser and phaser characteristics, new techniques to enhance the dispersion of the phasers as well as performance of the R-ASP system, depending on the applications are proposed in Chapter 2. Chapters 3 to 6 are the articles that introduce new applications of ASP. In Chapter 3, a novel loop technique to enhance the resolution of the phaser is proposed. In addition to frequency meters and frequency discriminators, this technique may readily by applied to various other real-time systems, such as real-time Fourier transformers, convolvers, correlators, and compressive radars. The radio-analog signal processing system has a lot of applications in the impulse regime. However, UWB pulse generation is complex and high cost. This issue is addressed in Chapter 4, proposing a low-cost analog pulse compression technique for UWB pulse generation. In Chapter 5, a stepped group delay phaser is introduced for real-time spectrum sniffing application. The system listens to its radio environment through an antenna, and determines, in real time, the presence or absence of active channels in this environment. The spectrum sniffer may find applications in cognitive radio systems. In Chapter 6, the concept of enhanced-SNR impulse radio transceiver

using phaser is demonstrated experimentally. Here, the SNR enhancement of the impulse radio is achieved for burst noise, Gaussian noise and low speed interferes. Chapter 7 discusses some more applications of the R-ASP. Finally, conclusions and future works are presented in Chapter 8.

TABLE OF CONTENTS

LIST OF TABLES

LIST OF FIGURES

LIST OF ABBREVIATIONS AND NOTATIONS

Abbreviations

1D:	One-dimensional
2D:	Two-dimensional
3D:	Three-dimensional
BPF:	Bandpass Filter
BPSK:	Binary Phase Shift Keying
BW:	Bandwidth
CMT:	Coupled-Mode Theory
CR:	Coupled-Resonator
CRLH:	Composite Right/Left-Handed
EM:	Electromagnetics
FBW:	Fractional Bandwidth
HPBW:	Half Power Beam Width
LH:	Left-Handed
LWA:	Leaky-wave Antenna
MoM:	Method of Moments
MTM:	Metamaterial
PCB:	Printed Circuit Board
PPM:	Pulse Position Modulation
QPSK:	Quadrature Phase Shift Keying
TCR:	Tapered Coupled-Resonator
TD:	Time Delayer
TEM:	Transverse Electromagnetic
TL:	Transmission Line
RH:	Right-Handed
UC:	Unit cell
UWB:	Ultra Wideband

Notations

c:	speed of light in vacuum $3 \cdot 10^8$m/s
ε_0:	permittivity of free space
μ_0:	permeability of free space
k_0:	free space wave number
λ:	wavelength
β:	propagation constant
$\vec{E}$:	electric field intensity
$\vec{D}$:	electric flux density
$\vec{H}$:	magnetic field intensity
$\vec{B}$:	magnetic flux density
Z_B:	Bloch impedance

LIST OF APPENDIX

CHAPTER 1 INTRODUCTION

1.1 Motivation

The recent explosion of data communication requirements in the microwave and wireless systems have led the radio and communication manufacturers to find new and innovative solutions to accommodate these ever growing system requirements. Wireless standards groups have employed all kinds of approaches to expand the capacity of today's communication networks, such as MIMO systems, dense cell communication networks, and smarter co-ordination between various devices. But none of these conventional techniques are capable of handling the foreseeable traffic flood expected in the next eight to ten years. According to MarketsandMarkets study, the next generation communication network will require an estimated 1000 fold increase in the capacity and system requirements. Consequently, the usage of large spectral bandwidth is inevitable in future wireless communications systems.

The state-of-the-art Digital Signal Processing (DSP) techniques have made outstanding advances into wireless and communication systems due to easy programmability, process flexibility, compactness, and reliability available with high-speed storage and computational circuits. However, DSP suffers of fundamental drawbacks, such as high cost of A/D and D/A converters, excessive power consumption and poor performance at high frequencies and broader bandwidths. Due to aforementioned problematics, the current digital techniques and solutions are not scalable to larger spectral bandwidth systems, specially at higher frequencies, and thus are unlikely to meet the challenging demands of future radio systems. Therefore, there is a pressing and an urgent need of devising disruptive technological solutions that transcend beyond conventional DSP techniques to solve the future crisis of massive data explosion.

Recently, a new signal processing paradigm has been proposed to offer a novel solution for new class of microwave and wireless system. This paradigm is termed Radio-Analog Signal Processing or R-ASP. R-ASP is emerging in microwave and millimeter-wave technology, where it may offer distinct benefits over conventional frequency-domain systems toward faster and broader bandwidth systems. In contrast with DSP, Analog Signal Processing (ASP) devices are innately frequency scalable, they are low power consumption since they don't need active logic circuits for processing, they are faster and less expensive because of their simple structure. Based on these considerations, radio systems based on ASP techniques have a potential to bring alternative solution to the DSP-based radios with particular promise to broadband applications, leading to systematic Radio-Analog Signal Processing (R-ASP).

1.1.1 Radio Analog Signal Processing

Radio ASP is the real-time operation, manipulation and analysis of radio signals in their original analog form without converting to the digital signal and using DSP devices. ASP devices have to manipulate the signals in the time-domain using engineered wave-propagation in dispersive microwave structures called phasers (proviously called DDS as an acronym for dispersive delay structure) [3] which is the core of an ASP system. In a phaser, the group velocity v_g is a function of the frequency, therefor each frequency component of the signal suffers from different delays following the delay versus frequency response of the phaser. The various spectral components of the signal can then be mapped into time domain and finally be processed in real time. Typical R-ASP applications include real-time spectrum analysis [4], spectrum sniffing [5], dispersion coding/decoding [6], frequency meter [2], pulse compression/decompression [7], chirp spread spectrum (CSS) [7]. R-ASP systems are inherently frequency scalable and thus can manipulate the signals directly at high frequencies without the need of down frequency conversion. In addition, they can easily be broadband, thereby capable of handing wide-band signals.

1.2 Thesis Contributions

The contribution of this thesis is two-fold: 1. Improving the dispersion capabilities of the phasers for high-resolution R-ASP. 2. Demonstration of new R-ASP systems.

1.2.1 Phaser and Dispersion Enhancement

Since phaser is the core of an ASP system, the performance of these systems is directly dependent on the performance of the phaser. Recently, conventional phasers are implemented in standard low-cost and frequency scalable microwave integrated circuit technologies, and they have already led to efficient real-time Fourier transformers [3,8], tunable pulse delay lines [9], ultra wideband modulators [10] and compressive receivers [11]. However, the performances of these phasers are limited by the maximal achievable group delay difference $\Delta\tau$ over the frequency band of operation Δf, i.e. the maximal delay difference and frequency difference product, $\Delta\tau \times \Delta f$, which define the frequency resolution of the phaser. In the first part of the thesis, novel techniques to enhance the dispersion of the phasers depending on the application using engineered structures and integrated components is presented.

1.2.2 R-ASP Applications

The prior applications of the radio-analog signal processing using phaser has been limited to tunable delay lines, pulse compression and Fourier transformation. The following applications for radio ASP has been conceptualized and demonstrated in this thesis.

1. Frequency discriminator/meter
2. Frequency sniffer
3. Enhanced SNR transceiver

1.3 Organization

This thesis is written in the format of articles. The details of the content of each Chapter is as follows

Chapter 2 Fundamentals of ASP

This Chapter focussed on phasers, which is the core of an ASP system ; it reviews phaser technologies, explains the characteristics of the most promising microwave phasers, and proposes corresponding enhancement techniques for higher ASP performance phaser design.

Chapter 3 Article 1: Increased Group Delay Slope Loop System for Enhanced-Resolution Analog Signal Processing

In this Chapter, a novel increased group delay slope loop scheme is proposed to enhance the time-frequency resolution of phasers for analog signal processing systems. This approach provides a solution to the unpractical approach of cascading n phaser units, which would lead to excessively large device footprint, unacceptably high insertion loss and severe signal-to-noise reduction.

Chapter 4 Article 2: Low-Cost Analog Pulse Compression Technique based on Mixing with an Auxiliary Pulse

A pulse compression technique to generate UWB pulses for using in ASP systems is proposed in this Chapter. This technique consists in multiplying the pulse to compress with an auxiliary baseband gaussian pulse, which results in a compression of $\sqrt{2}$, and re-injecting this pulse n times around a loop including an amplifier, a delay line and an isolator, so as to achieve a compression factor of $\sqrt{1+n}$.

Chapter 5 Article 3: Distortion-less Real-Time Spectrum Sniffing Based on a Stepped Group-Delay Phaser

In this Chapter, the idea of frequency sniffing, based on the real-time frequency discrimination enabled by a stepped group-delay phaser is introduced. Functionally, the system listens to its radio environment through an omnidirectional antenna, and determines, in real time, the presence or absence of active channels in this environment so as to allow an associated communication system to opportunistically reconfigure itself to transmit in the available bands in a cognitive radio sense.

Chapter 6 Article 4: Enhanced-SNR Impulse Radio Transceiver based on Phasers

In this Chapter, the concept of the enhanced-SNR in impulse radio transceiver using phasers of opposite chirping slopes is proposed. It has been shown that SNR enhancement by factors M^2 and M are achieved for burst noise and Gaussian noise, respectively, where M is the stretching factor of the phasers. The transceiver system is simple, low-cost and frequency scalable, and may therefore be suitable for broadband impulse radio ranging and communication applications.

Chapter 7 General Discussion

This Chapter shows R-ASP application classification and addresses some more applications of the R-ASP such as, FDM demodulation and frequency sector detection.

Chapter 8 Conclusions and Future Works

CHAPTER 2 FUNDAMENTALS OF ANALOG SIGNAL PROCESSING

This Chapter introduces the concept of ASP in context of dispersion and presents the phaser as core of an ASP system ; it reviews phaser technologies, explains the characteristics of the most promising microwave phasers up-to-date, and proposes corresponding enhancement techniques for higher performance phaser in the ASP systems.

2.1 ASP Concepts

The basic principle of a ASP maybe understood from Fig. 2.1 based on two basic operations of a phaser [1] on a time-domain input pulse: chirping and frequency discrimination. A phaser is here represents an electromagnetic signal processor that produces specified frequency sweeping effect in real time. Chirping and frequency discrimination maybe obtained by passing a pulse through a phaser with transfer function $H(\omega) = e^{j\phi(\omega)}$ with a unity amplitude and whose phase, $\phi(\omega)$ is a nonlinear function of frequency, or whose group delay, $\tau(\omega) = \partial\phi(\omega)/\partial\omega$, is a function of frequency.

In the chirping case, shown in Fig. 2.1(a), a quasi-Gaussian pulse modulated at an angular frequency, ω_0 is injected into the phaser $H(\omega)$ with a positive linear group delay covering the input pulse bandwidth centered at the frequency ω_0. The different frequency components of the output pulse are delayed due to the dispersive nature of the phaser. Here, the lower frequency components are less delayed, so the output signal has a progressive instantaneous frequency. This phenomenon causes time spreading ($T_{\text{out}} > T_0$) accompanied by amplitude reduction due to energy conservation. If a chirped pulse passes through a phaser with an opposite group delay slope, the output pulse will be compressed along with the recovery of the amplitude of the original pulse. Pulse compression [12], compressive receivers [11], real-time Fourier transformation [4, 13],impulse radio SNR enhancement [14], and chirp spread spectrum (CSS) encoding [7, 15] are some of the examples of chirping applications in R-ASP.

In the second case, shown in Fig. 2.1(b), the input pulse is two tone signal with ω_1 and ω_2 frequencies inputs through the phaser $H(\omega)$ with a positive two step group delay, centered at ω_1 and ω_2, corresponding to group delays τ_1 and τ_2, respectively. The output signal contains two pulses centered at frequencies ω_1 and ω_2 which are delayed by τ_1 and τ_2, respectively based on the phaser dispersion characteristic. Here, the pulses are not time-spread ($T_{out} = T_o$) due to the flat group delay response of the phaser where the pulses bandwidth fit in the non-

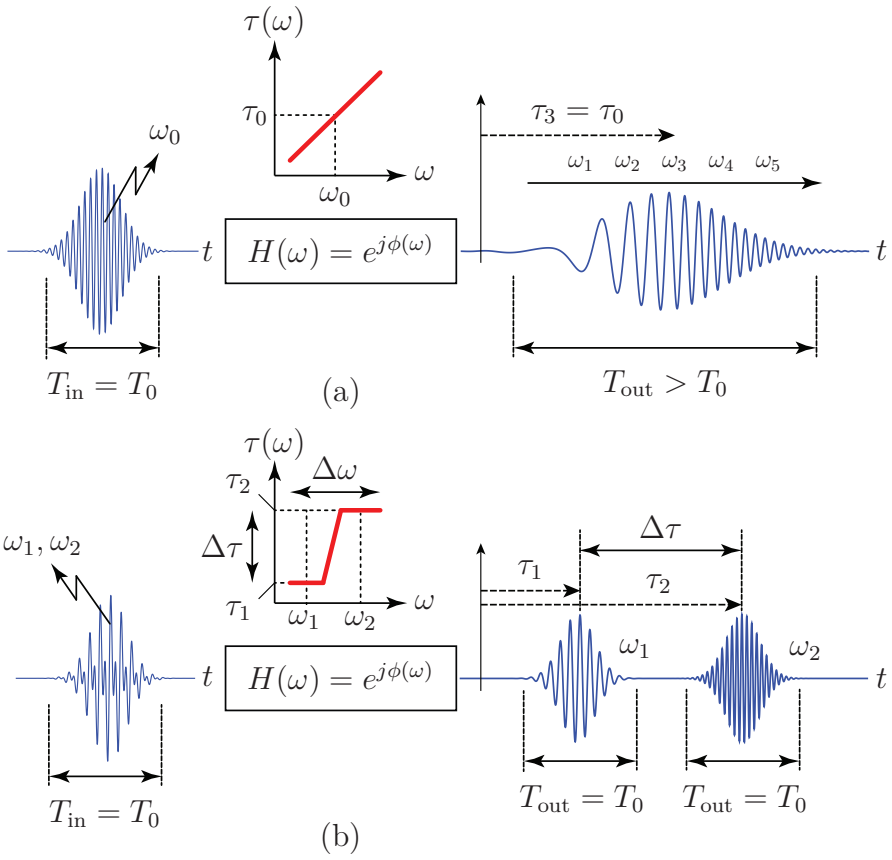

Figure 2.1 Essential effects in ASP. (a) Chirping. (b) Frequency discrimination. Figure has been reproduced from [1].

dispersive bands of the delay steps. This is the concept of frequency discrimination which is used for frequency division multiplexing (FDM) [16] and frequency sniffing [5] in R-ASP applications.

2.2 Phaser as the Core of an ASP System

An ideal phaser with an arbitrary group delay and flat lossless magnitude over a given frequency band is shown in Fig. 2.2. The goal of the phaser synthesis and design [17] is to obtain a phaser response as close as possible to this ideal phaser where the magnitude response is flat in the passband and the delay response is the specified delay function to accomplish a specific R-ASP application.

The Taylor expansion of the phase response around the center frequency of the phaser band-

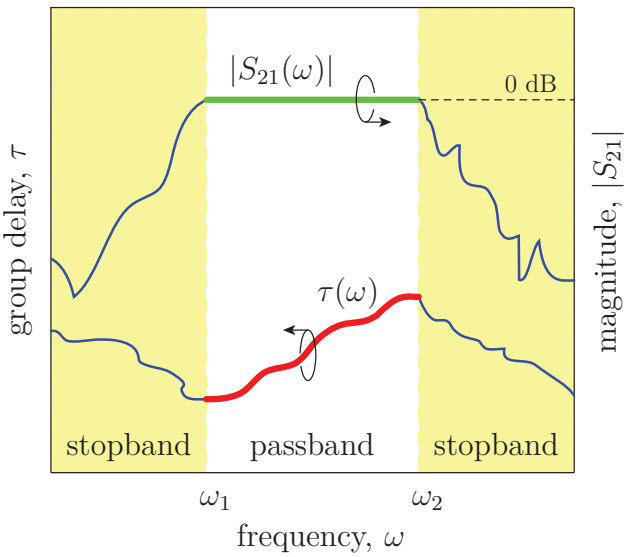

Figure 2.2 An arbitrary group delay with flat lossless magnitude response. Figure has been reproduced from [1].

width, ω_0 is

$$\phi(\omega) = \phi_0 + \phi_1(\omega - \omega_0) + \frac{\phi_2}{2}(\omega - \omega_0)^2 + \frac{\phi_3}{6}(\omega - \omega_0)^3 + \dots \tag{2.1a}$$

$$\text{with} \quad \phi_k = \left.\frac{\partial^k \phi(\omega)}{\partial \omega^k}\right|_{\omega=\omega_0}. \tag{2.1b}$$

where $\phi_0 = \phi_(\omega_0)$, $\phi_1 = -\tau(\omega_0)$ and $\phi_2 = \left.\frac{\partial \tau}{\partial \omega}\right|_{\omega_0}$ are phase delay parameter, group delay parameter and group delay slope parameter, respectively.

The group delay of the phaser is obtained from (2.1a) as

$$\tau(\omega) = \frac{\partial \phi(\omega)}{\partial \omega} = \phi_1 + \phi_2(\omega - \omega_0) + \frac{\phi_3}{2}(\omega - \omega_0)^2 + \dots, \tag{2.2}$$

Various analog signal processing applications require different delay versus frequency response. For instance, if $\phi_2 \neq 0$ with $\phi_k = 0$ for $k > 2$, the group delay response of the phaser is linear. The linear group delay response is used for Fourier transformers and pulse compressors. On the other hand, applications such a dispersion compensators and frequency sniffers may need a higher order dispersion terms.

Phasers for analog signal processing applications can be designed in various technologies. Figure 2.3 shows some of the most common microwave phasers. A high dispersion medium

device with a larger bandwidth can be implemented by a linearly chirped Bragg coupling between the quasi-TEM micro-strip mode, Fig. 2.3(a,b). This is achieved by varying continuously the impedance of the line either by altering the strip width or by etching the line ground plane. This approach is simple, and can achieve large delay swings in a larger frequency band. However, the group delay responses of such Bragg structures exhibits large unwanted delay ripples, requiring more sophisticated designs to smoothen these ripples. Figure 2.3(c) shows the waveguide-implementation for coupled-resonator phasers. The biggest drawback of all these structures is the need of a circulator to separate the input and output signals.

MSW technology, Fig. 2.3(d) was used for phaser design since 1980. Magnetostatic waves (MSW) [18] are slow waves that can propagate in ferri- or ferromagnetic materials at microwave frequencies and have potential application in compact microwave signal-processing devices used in radar, electronic warefare, and communication systems. Demonstrated MSW devices include dispersive and constant delay lines, filters and filter banks, correlators and convolvers, as well as non-linear devices such as signal to noise enhancers and frequency-selective limiters. Their unique features, compared with other signal-processing technologies such as surface acoustic waves (SAW), include operation directly at microwave frequencies and tunability via the magnetic bias field.

A surface acoustic wave (SAW) [19], shown in Fig. 2.3(e) is an acoustic wave traveling along the surface of a piezoelectric material, with an amplitude that typically decays exponentially with depth into the substrate. When a time varying voltage is applied to the input transducer, the periodic electric field induces a corresponding elastic stress in the piezoelectric material. Surface waves are generated strongly for frequencies with wavelengths similar to the transducer pitch. At the output, the receiving transducer acts in a reciprocal manner, converting incident acoustic waves to an output voltage. Thus, the device converts an electrical input signal into an electrical output signal. Typically, a transducer might have 20-1000 electrodes. The electrode spacing is a quarter of the center-frequency wavelength, the minimum possible spacing, determined by the fabrication technology, limits the frequency obtainable. In commercial production, the minimum width is about 0.5 μm. For a typical acoustic wave velocity of 3000 m/s this gives a maximum operating frequency of 1.5 GHz, though special techniques can extend this to 5 GHz. As such, high frequency signals must be down converted to make use of SAW devices. Composite right/left-handed (CRLH) transmission lines [Fig. 2.3(f)] may have their dispersion controlled in terms of the Taylor coefficients of their wave number, under the constraint of fixed Bloch impedance for broadband matching [9, 11, 20]. They are less compact than MSW-based and SAW-based phasers, but they may be scaled to higher frequency.

Reflection-type phasers

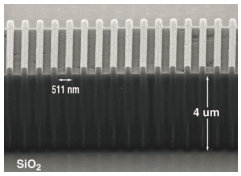

(a) optical Bragg grating [21]

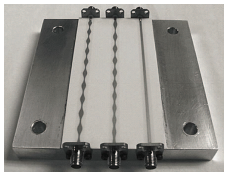

(b) chirped microstrip line [22]

(c) coupled-resonator structure [23]

Transmission-type phasers

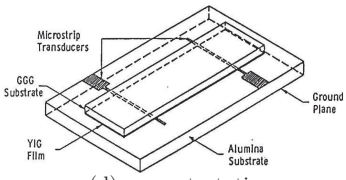

(d) magnetostatic wave device [24]

(e) surface acoustic wave device [25]

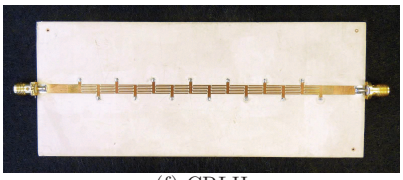

(f) CRLH transmission line [26]

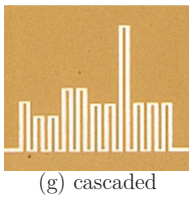

(g) cascaded C-section structure [3]

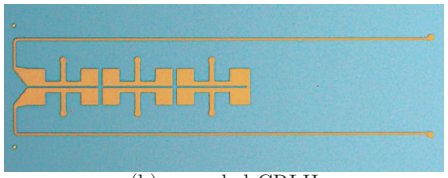

(h) cascaded CRLH C-section structure [20]

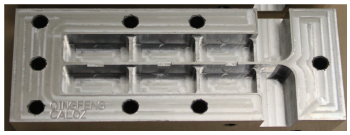

(i) cross-coupled resonator structure [17]

Figure 2.3 Some of the most common microwave phasers.

Cascaded C-section structure phasers [3, 27] are two-port structures based on coupled transmission lines as shown in Fig. 2.3(g). A C-section is a 2-port network obtained by connecting a short transmission line to the two end ports of a coupled-line coupler. Its transfer function and the group delay response are given by

$$S_{21}(\theta) = \frac{\sqrt{1+k\cos\theta} - j\sqrt{1-k\sin\theta}}{\sqrt{1+k\cos\theta} + j\sqrt{1-k\sin\theta}}, \tag{2.3}$$

$$\tau(\theta) = \frac{2a}{a^2 + (1-a^2)\cos^2(\theta)}\frac{d\theta}{d\omega}, \text{ with } a = \sqrt{\frac{1-k}{1+k}}, \tag{2.4}$$

where $\theta = \beta l$ with $l = \lambda g/4$ at the frequency of the delay peak, where k is the coupling coefficient of the coupler, and β is the propagation constant of the transmission line elements of the coupler. It may be easily verified that this function satisfies the magnitude condition $|S21(\theta)| = 1$ of an all-pass response. The typical group delay response of a C-section is

shown in Fig. 2.4(b). This response is periodic in frequency and exhibits delay peaks at $\lambda = (2m + 1)\lambda_g/4$, where m is an integer. Cascading C-sections of different lengths forms with group delay responses represented by the colored curves in Fig. 2.4(b) results a total group delay response whose the delay at each frequency is the sum of the delays incurred by each C-section, as represented by the black curve in Fig. 2.4(b).

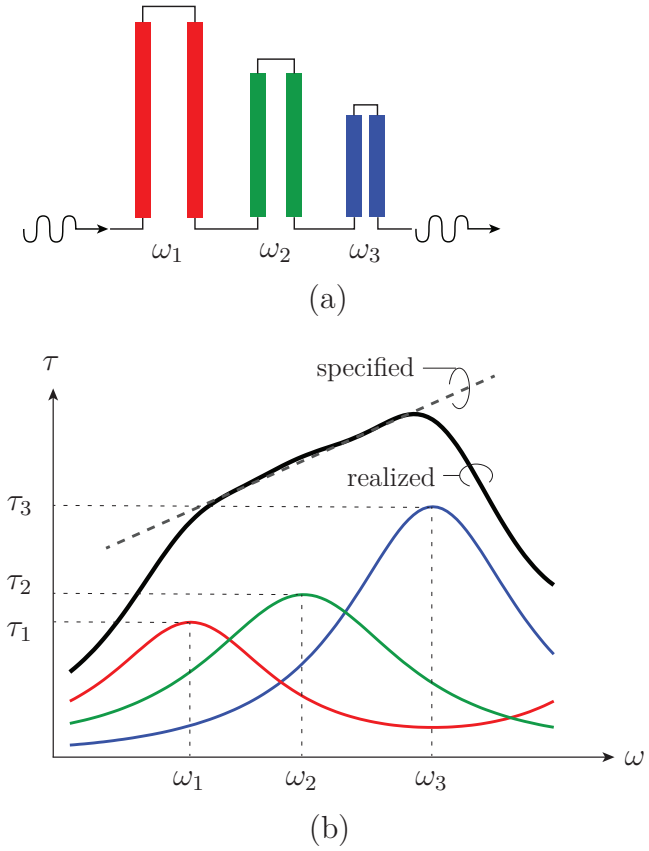

Figure 2.4 Principles of the C-section phaser. (a) Three Cascaded C-section elements [Fig. 2.3(g)] with different lengths. (b) Group delay response formation for (a). Figure has been reproduced from [1].

While, coupled-resonator phasers [Fig. 2.3(c)], cascaded C-section phasers [Fig. 2.3(g)], and cross-coupled resonator phasers [Fig. 2.3(i)], seem the most promising technologies for ASP systems, artificial (e.g., CRLH) transmission line phasers seem the best option for radiated and spatially dispersive phasers. High-resolution ASP systems require phasers with large dispersion or group delay swings. This issue of phaser characteristics influencing the performance of an ASP system and the some potential solutions to overcome them are described next.

2.3 Phaser Characteristics and Enhancement

The enhancement of the phaser characteristics increases the performance of the ASP systems. The resolution, the absolute bandwidth, and the magnitude balance are three important phaser characteristics.

The concept of the resolution characteristic can be understood from Fig. 2.1(b), which shows a frequency discriminator as one of the ASP applications. If the group delay difference, $\Delta\tau$ of the phaser response over the frequencies ω_1 and ω_2 is not large enough, the pulses will not be enough discriminated at the output of the phaser. This indicates the resolution of the system is proportional to the group delay difference over center frequencies of the modulated pulses. Moreover, if the pulse duration, T_0 is reduced, the two output pulse will be well discriminated. Hence, the resolution of an ASP system ϱ, should follow $\varrho \propto \Delta\tau/T_0$ or similarly, $\varrho \propto \Delta\tau B_0$, where B_0 is the bandwidth of the input pulse.

In order to increase the resolution of an ASP system, the group-delay swing of the phaser that it utilizes should be increased. This can be achieved using a brute-force approach by cascading a large number of phasers. This approach leads to an unacceptable high insertion loss preventing signal detection in the presence of the noise. Figure 2.5(a) represents a technique to enhance the ASP resolution by using a feedback loop circuit. In this system, the signal at the output of the phaser, $y_N(t)$ is regenerated by an amplifier and re-injected via a non-dispersive delay line toward its input along a loop. At each pass across the phaser, the effective group delay slope of the system is increased, so that after N turns along the loop the time-frequency resolution has been enhanced by a factor N. So, the resolution has been multiplied by the same factor. Figure 2.5(b) shows the group delay slope of the system which is progressively increased as the signal loops in the system. This technique and its applications will be discussed in Chapter 3. Usage of the feedback technique solves the problem of limited microwave phaser resolution in much more efficient manner.

The required absolute bandwidth and group delay of the phaser vary based on the applications. For instance, the absolute bandwidth of the phaser in frequency sniffer which will be discussed in Chapter 5 is 9 GHz with 3.5 nsec group delay swing. In frequency sniffer application where the absolute bandwidth is 9 MHz the group delay swing should be much more bigger, so 3.5 nsec group delay may be much more insufficient. In this case, another phaser technology such as reflection-type coupled-resonator [23] must be used. Where the relevant frequency bandwidth is very small in some applications, the absolute frequency bandwidth of the phaser will be an essential figure of merit.

The third characteristic of the phaser is magnitude balance. Magnitude balance is defined

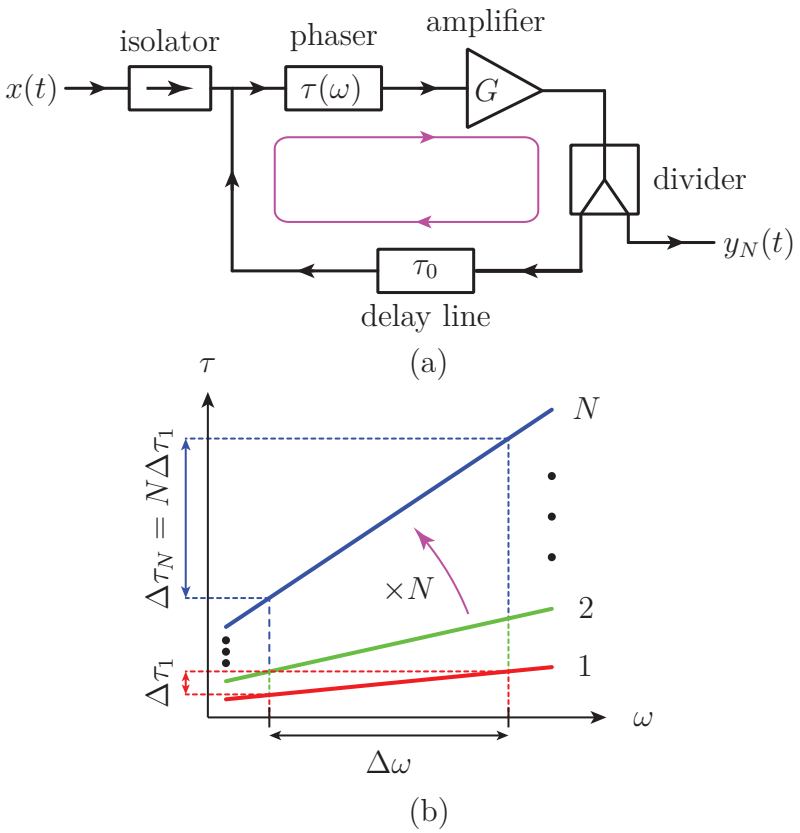

Figure 2.5 Loop resolution enhancement principle [2]. (a) Circuit block diagram. (b) Group delay slope ($|\phi_2|$) multiplication.

as the flat insertion loss, S_{21} over the bandwidth of the transmission phaser which is the characteristic of the ideal phaser as shown in Fig. 2.2. In the real case, the insertion loss of the phaser is not flat due to frequency dependent dielectric and conductor losses. Compared to the total amount of losses, which can be compensated using loop architectures, a non-flat transmission response poses serious difficulties such as signal distortions in ASP techniques. Therefore, transmission phasers require an amplitude equalization network to compensate non-flatness magnitude [28]. We will see how magnitude imbalance comes about, how it affects ASP, and how to remedy it for higher ASP performance in "System Problematic" section.

2.4 Phaser Synthesis

The goal of phaser synthesis is to obtain a response as close as possible to the ideal response shown in Fig. 2.2. So, the phaser resolution must be adequately high, its insertion loss must be flat, and its absolute bandwidth should be convenient for the intended application. The

shape of the phaser response is mostly linear, as required for instance in RTFT and pulse compressors, but it may be quadratic, cubic based on the application. The phaser response can also be more complex as stepped group delay response used in spectrum sniffer to be presented in Chapter 5.

A synthesis of the the C-Sections network phaser has been well presented in the article [3]. In this synthesis, the arbitrary group-delay response is achieved by combining the group-delay responses of C-sections with different lengths. Moreover, a computer design approach based on genetic algorithms is applied in this synthesis, which consists of determining the structural parameters of the different C-section groups.

A systematic synthesis method for cross-coupled phasers with controlled magnitude for ASP applications has been introduced in the article [17]. The transfer function is synthesized using a polynomial expansion approach, which allows to separately control the magnitude and group-delay response of the phaser.

The concept of space mapping has been applied for the first time in the article [27], to design a phaser using coupled C-sections. The results indicate that the space mapping synthesis technique for phaser design is more accurate and the implementation is simple compared to generic algorithms synthesis, presented in [3].

The synthesis of narrowband reflection-type phasers with arbitrary prescribed group delay has been presented in the article [29]. A high group-delay swing at a narrow frequency band is achievable using this technique.

2.5 System Problematic

There is a big demand for high resolution systems in the ASP applications, such as frequency sniffing and real-time FDM modulation [16]. The cascading of the phasers is a common approach for resolution enhancement. However, the resulting system would be large, and would suffer from high insertion loss. Moreover, The system would have a poor signal-to-noise due to the low level of the signal reaching the amplifier in the end of the phaser. One solution may be using a lower loss dielectric and conductor material in phaser design but that increases the overall cost of the phaser. Another solution is loop feedback system which is presented in Chapter 3.

When a broadband pulses are injected to a phaser, the output pulses will be time-spread because of dispersive characteristic of the phaser. The larger pulse bandwidth results a wider pulse in time. So, the resolution of the system is decreased. Chapter 5 presents a stepped group delay pahser design where the a multiple channel input is discriminated in time domain,

where each channel occupies a non-dispersive frequency band.

A phaser has a non-flat insertion loss, based on frequency dependent dielecteric loss, $\alpha_d \propto \omega$ and conductor loss, $\alpha_c \propto \sqrt{\omega}$. This non-flat response leads the system to distort the input signal by an attenuation factor, $e^{-\alpha_m(\omega)l} = e^{-(\alpha_c(\omega)+\alpha_d(\omega))l}$, where l is effective length of the phaser. The attenuation factor strongly depends on frequency, and increases with frequency in an up-chirp phaser, and may decrease in some delay desings with frequency in a down-chirp phaser, shown in Fig. 2.6. Once solution to overcome this issue is the equalization of the amplitude by an equalizer circuit with an opposite slope insertion loss [30].

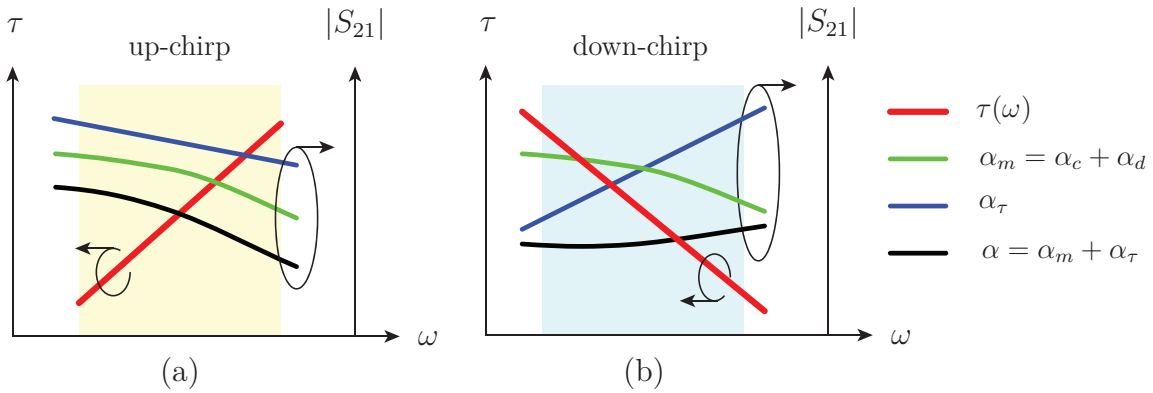

Figure 2.6 Magnitude imbalance due to the loss in a phaser. (a) Material and dispersion losses for an up-chirp phaser. (b) Material and dispersion losses for a down-chirp phaser.

R-ASP system has a lot of applications in the impulse regime. Pulse compressors and stretchers, pulse radar, UWB systems, and impulse radios are example for R-ASP applications. Also, UWB pulses are the important part of the R-ASP systems in impulse regime. UWB pulse generation technique mostly uses digital and CMOS technique which is expensive and high power consumption. A new low-cost analog technique for UWB pulse generation based on mixing with an auxiliary pulse are presented in Chapter 4.

Finally, a phaser with the millimeter-wave frequency range is highly desired for ultra high speed ASP applications. However, the fabrication limitation and high insertion loss of the conventional phasers at millimeter-wave frequencies limit their usage for millimeter-wave applications. So, more research and development in this area is needed. Since the insertion loss and the spectral bandwidth of the wave guide transmission lines at high frequency are much better than printed circuit boards (PCB) (i.e. microstrip and stripline), they may be good candidates as an alternative technology for future phaser design. Similarly, the coplanar waveguide technology maybe more suitbale for PCB based phaser design.

CHAPTER 3 ARTICLE 1: INCREASED GROUP-DELAY SLOPE LOOP SYSTEM FOR ENHANCED-RESOLUTION ANALOG SIGNAL PROCESSING

Babak Nikfal, Shulabh Gupta, and Christophe Caloz

IEEE Trans. Microwave Theory Tech., vol. 59, no. 6, pp. 1622-1628, Jun. 2011.

A novel increased group delay slope loop scheme is proposed to enhance the time-frequency resolution of dispersive delay structure (DDS) components for microwave analog signal processing systems. In this scheme, the signal at the output of the DDS is regenerated by an amplifier and re-injected via a non-dispersive delay line toward its input along a loop. At each pass across the DDS, the effective group delay slope of the system is increased, so that after n turns along the loop the time-frequency resolution has been enhanced by a factor n. This approach provides a solution to the unpractical approach of cascading n DDS units, which would lead to excessively large device footprint, unacceptably high insertion loss and severe signal-to-noise reduction. The proposed scheme is implemented in a proof-of-concept circuit using a C-section all-pass network DDS and demonstrated experimentally in a frequency meter and in a frequency discriminator. Possible improvements for higher performance are discussed.

3.1 Introduction

Temporal (as opposed to spatial) frequency dispersion is the property according to which a material delays the different time spectral components of a modulated signal by different amounts of time [31]. This effect is commonly used at both optical [32] and radio [33] frequencies for analog signal processing, i.e. for the real and continuous time manipulation of broadband signals, with particular benefit for low-complexity and high-speed instrumentation and communication systems [34]. Although it has been less applied in microwave components, mainly due to the difficulty of realizing efficient dispersive delay structures (DDS) in the corresponding frequency range, dispersion engineering has a great potential in this area to address new challenges in faster, higher frequency and more reconfigurable circuits, using various real-time systems, such as frequency meters and discriminators, real-time Fourier transformers, convolvers, correlators and compressive radars [33–35].

Over the past few decades, several microwave technologies have been explored for DDSs, including surface acoustic wave (SAW) [19, 34], magnetostatic wave (MSW) [18, 36], super-

conducting cascaded coupler [37], chirped transmission line [15, 38], metamaterial structure [39, 40] and all-pass network [3, 13] technologies, all exhibiting different merits and drawbacks. SAW, MSW and superconductive technologies are not well amenable to several microwave DDS applications due to restricted maximal frequency, biasing magnet requirement and cryogenic constraint, respectively. In contrast, more recent chirped transmission lines, metamaterial and all-pass network DDSs are implemented in standard low-cost and frequency-scalable microwave integrated circuit technologies, and they have already led to efficient real-time Fourier transformers [3, 8], tunable pulse delay lines [9], ultra wideband modulators [10] and compressive receivers [11]. However, the performances of these DDS systems are limited by the maximal achievable group delay difference $\Delta\tau$ over the frequency band of operation Δf, i.e. the maximal delay difference and frequency difference product, $\Delta\tau \times \Delta f$, which define the time-frequency resolution and bandwidth, respectively, of the system.

In order to achieve a large $\Delta\tau \times \Delta f$ product to maximize the time-frequency resolution of analog signal processors, several approaches can be followed. The simplest technique is to cascade a large number of DDSs, as shown in Fig. 4.1(a), until the required group delay difference has been reached. However, this approach is practically unrealistic as it leads to an excessively large device footprint and to unacceptably high insertion loss, preventing signal detection in the presence of parasitics and noise. The losses in the structure may be conceptually compensated by using an amplifier with a high gain. However, this is an expensive device. Moreover, if the amplifier is placed at the end of the cascade, both the useful and the unwanted parasitic signal are amplified, which makes detection problematic ; if placed at the front of the cascade, the amplifier will typically saturate. In either case, using a high-gain amplifier severely restricts the performance of the system. This requirement for a high gain amplifier may be alleviated by using a distributed amplification scheme, as illustrated in Fig. 4.1(b). This approach relaxes the high gain constraints of the amplifier at the cost of requiring a large number of devices, which in turns leads to high power consumption, high cost and high biasing circuit complexity. In addition, both schemes, in order to provide a total group delay swing of $n\Delta\tau$, require n DDS units, n amplifiers and n other circuit components such as matching sections and biasing networks, which naturally results in larger size, high system cost and high complexity. Therefore, the cascading approach becomes impractical when a large group delay swing is required.

Compared to these techniques, this paper solves the problem of limited microwave DDS resolution in a much more efficient manner by using a novel DDS loop scheme. The proposed scheme enhances the resolution of any DDS by passing the signal several times across it and regenerating it by amplifying it after each pass, as illustrated in Fig. 4.1(c). The proposed

loop system is compact in size and requires only one set of circuit components, i.e. DDS, amplifier, matching section and biasing network, resulting in lower power consumption and lower system cost, compared to the two aforementioned cascading schemes. In addition, the proposed system is highly flexible in achieving variable amounts of group delay swing by simply controlling the number of turns in the loop (for instance using a switch and a counter), which is not possible in the cascading approach. This makes the system versatile and suitable for various applications requiring different amounts of group delay swings.

The paper is organized as follows. Sec. 3.2 describes the principle of the proposed DDS loop system. Sec. 3.3 presents its prototype implementation using a C-section all-pass network as the DDS, and demonstrates two subsequent applications: a frequency meter [41, 42] and a frequency discriminator [43, 44]. Sec. 3.4 discusses possible improvements of these proof-of-concept demonstrations. Finally, conclusions are given in Sec. 3.5.

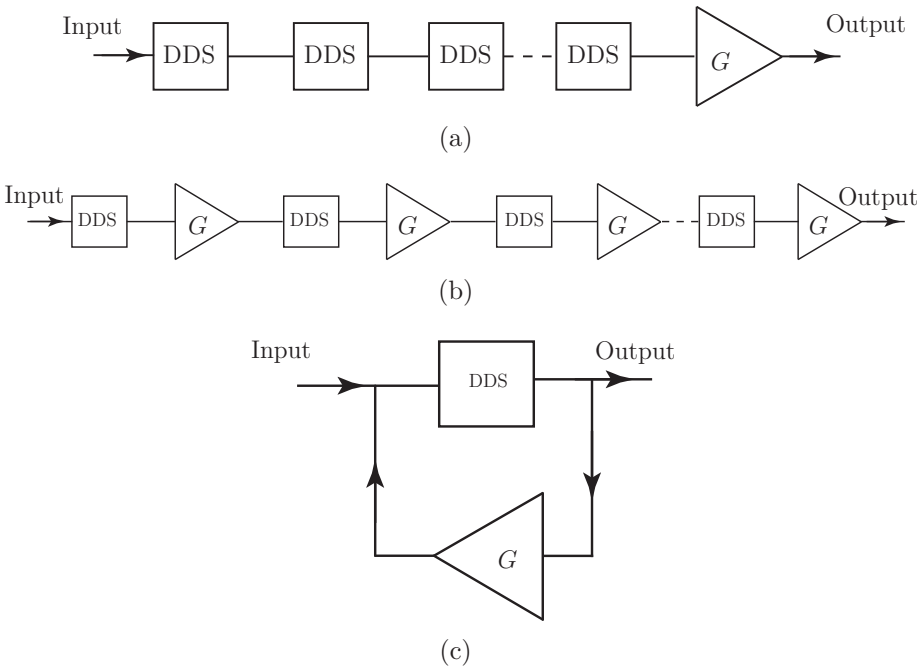

Figure 3.1 Different possible techniques for increasing the group delay swing of a dispersive delay structure (DDS). (a) Cascaded DDSs with a single amplifier. (b) Cascaded DDSs with distributed amplification. c) Proposed loop technique.

3.2 Principle

Fig. 3.2(a) shows a simplified schematic of the system, which essentially consists of a loop, placed between the input and output ports and including a DDS with a group delay response

$\tau(\omega)$, an amplifier, a frequency-independent (non-dispersive) delay line of delay τ_0 and a power divider.

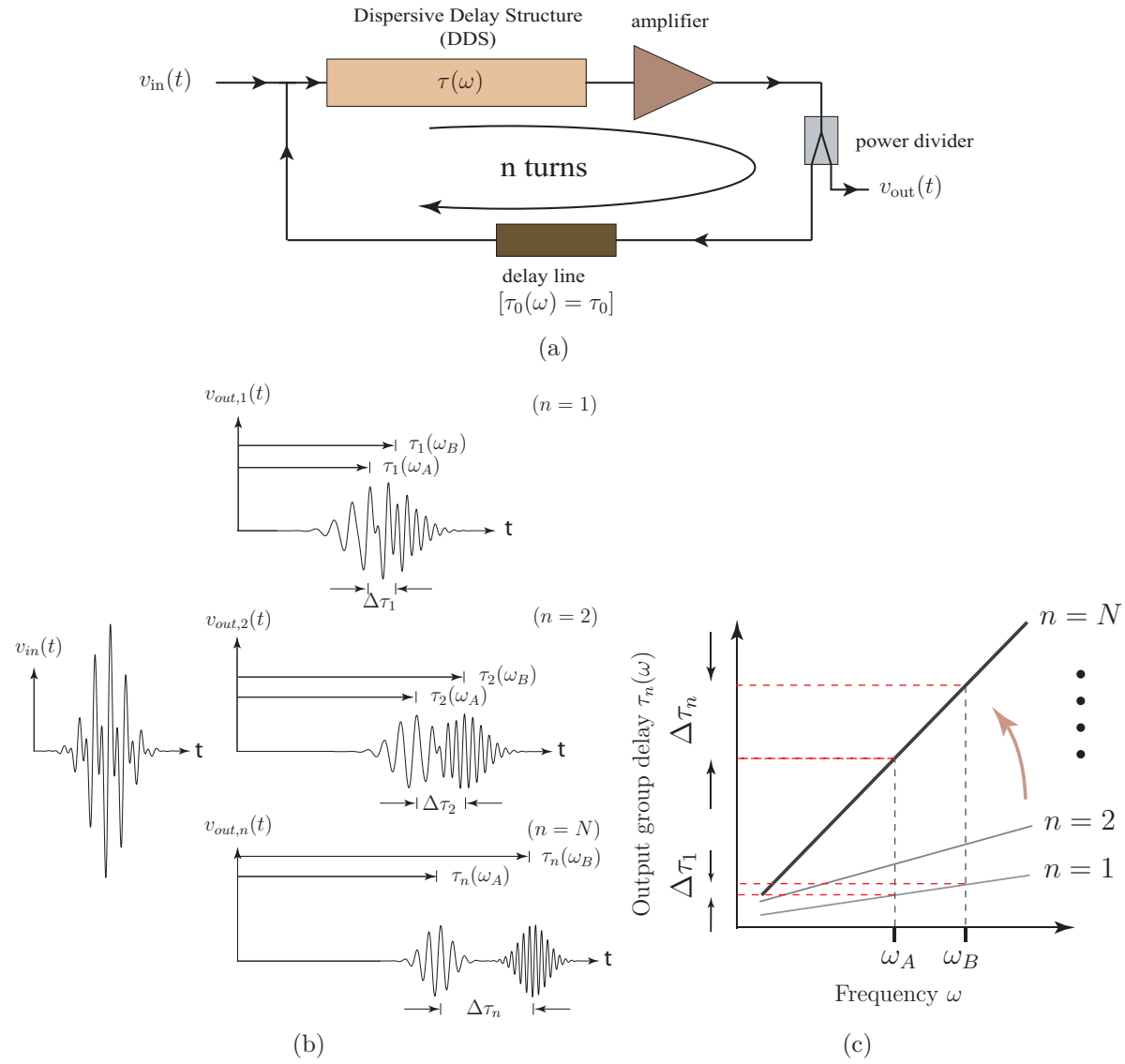

Figure 3.2 Principle of the proposed increased group delay slope system. (a) Schematic. (b) Illustration of enhanced time resolution with increased number of turns for the case of an input gaussian pulse modulated with two carrier frequencies ω_A and ω_B. (c) Slope enhancement, providing an n-fold increased resolution [s_n in (3.2)] for analog signal processors.

The essential function of the loop is to enhance the group delay difference in a given frequency range from the amount provided by the single DDS, $\Delta\tau$, to $n \times \Delta\tau$, by passing the input signal n times into the DDS. This group delay enhancement subsequently increases, by the same factor n, the real-time frequency resolution of analog signal processors.

Let us consider an input signal $v_{in}(t)$ constituted by a single pulse $v_0(t)$ modulated with two carrier frequencies ω_A and ω_B, respectively, i.e. $v_{in}(t) = v_{in,A}(t) + v_{in,B}(t) = v_0(t)\sin(\omega_A t) + v_0(t)\sin(\omega_B t)$.

First, $v_{in}(t)$ is injected into the loop. At the first pass across the DDS ($n = 1$), the A and B spectral components of the signal, due to their different group delays incurred by the DDS, are separated in time by the amount $\Delta\tau_1 = \tau(\omega_B) - \tau(\omega_A)$ within the frequency range $[\omega_A, \omega_B]$, as shown in Fig. 3.2(b). The amplifier compensates for the losses introduced by the DDS and by the other elements of the loop. The resulting signal, with time separated pulses, is then split by a power divider. Part of it becomes the first pulse $v_{out,1}(t)$ of the output signal, $v_{out}(t)$, while the other part is re-injected toward the input of the DDS via the non-dispersive delay line. After the second pass across the DDS ($n = 2$), the time separation between the A and B components of the signal is doubled, i.e. $\Delta\tau_2 = 2\Delta\tau_1$, as shown in Fig. 3.2(b). This is the same thing as saying that the group delay slope of the system, or equivalent group delay slope, has doubled, within the same frequency range.

Thus, the effective $\Delta\tau \times \Delta f$ product of the system has doubled. As before, the amplified signal, with its A and B components now twice further apart in time, is split by the power divider to build for one part $v_{out,2}$ and to be for the other part re-injected into the system. And the cycle continues, so that after n turns around the loop, the A and B components of the input signal have been resolved in the output signal $v_{out,n}$ by a time separation of $\Delta\tau_n = n\Delta\tau_1$, as shown in Fig. 3.2(b).

The $\Delta\tau \times \Delta f$ product has thus increased by a factor n. The explanation just given for a two-tone modulation can be straightforwardly extended to the case of a broadband signal including a continuum of frequencies across the bandwidth of the DDS, for which the system can operate as a real-time Fourier transformer if sufficient dispersion is available [13, 15].

The role of the non-dispersive delay line is to avoid self-overlapping of the pulse traveling around the loop, i.e. the superposition of its trailing part entering the DDS and of its leading part exiting the DDS. To avoid such overlap, the condition $\Delta\ell/v_g > \Delta T$ must be satisfied, where $\Delta\ell$ is the length of the DDS, ΔT is the time duration of the pulse and v_g is the group velocity the DDS. As this condition is generally not satisfied from the DDS only, the additional delay τ_0 of the non-dispersive delay line is used to provide the overlap avoidance condition $\Delta\ell/v_g + \tau_0 > \Delta T$. In practice, a slightly larger τ_0 value is required to take into account the time spreading effects due to dispersion. The additional delays due to the other components of the loop (e.g. amplifier and matching elements) may be absorbed in the delay τ_0.

In summary, the total group delay for the system of Fig. 3.2 after n turns is

$$\tau_n(\omega) = n\tau(\omega) + (n-1)\tau_0, \tag{3.1}$$

which corresponds to the group delay versus frequency slope

$$s_n = \frac{d\tau_n(\omega)}{d\omega} = n\frac{d\tau(\omega)}{d\omega} = ns_1, \tag{3.2}$$

where s_1 corresponds to the slope of the isolated DDS. As will be seen later, s_n is the time-frequency resolution of the system, i.e. its frequency resolution obtained from the time domain.

At this stage, it is important to differentiate the proposed loop system from a conventional feedback system operated in the continuous wave regime. In contrast to such a system, the proposed loop system operates in the impulse regime. Due to this regime, the traveling pulsed signal never overlaps with itself. The presence of the delay element of constant delay τ_0 in the loop ensures this condition by delaying the pulse enough so as to avoid any overlap between its leading and trailing edges. Maintaining in addition the loop gain always smaller than unity within the operation frequency band of the DDS, thereby avoiding the Barkhausen oscillation criterion [45], ensures the stability of the system. In practice, the loop system could potentially oscillate due to parasitic signals outside the frequency band of operation. However, this issue can be easily avoided by placing a bandpass filter in the loop. In this case, the DDS must be co-designed with the filter and specifically take into account its group delay response, in particular near the cutoff frequencies, which can be systematically achieved by using non-commensurate all-pass networks [3].

3.3 Experimental Demonstration

3.3.1 C-Section Implementation

For the sake of illustration of the proposed increased group delay slope system, we shall consider an implementation using a C-section network as the DDS [3]. This DDS is a planar version of the all-pass filter [30, 46] introduced by Hewitt in [47], and extended in [3] for the systematic design of quasi arbitrary group delay responses. Fig. 3.3 presents the measured response for a commensurate (all C-sections with same length) microstrip C-section all-pass network, which will be used in the system prototype shown in Fig. 3.4(a). Non-commensurate C-section networks with other desired group delay profiles and slope signs [3] could have been chosen. Fig. 3.3(b) shows the S-parameters while Fig. 3.3(c) shows the group delay response of the DDS. The length of the C-section network has been restricted so as to avoid excessive

insertion loss and mismatch while still providing a substantial time-frequency resolution, here $\Delta\tau = 4.5$ ns within the 0.3-1.0 GHz frequency range.

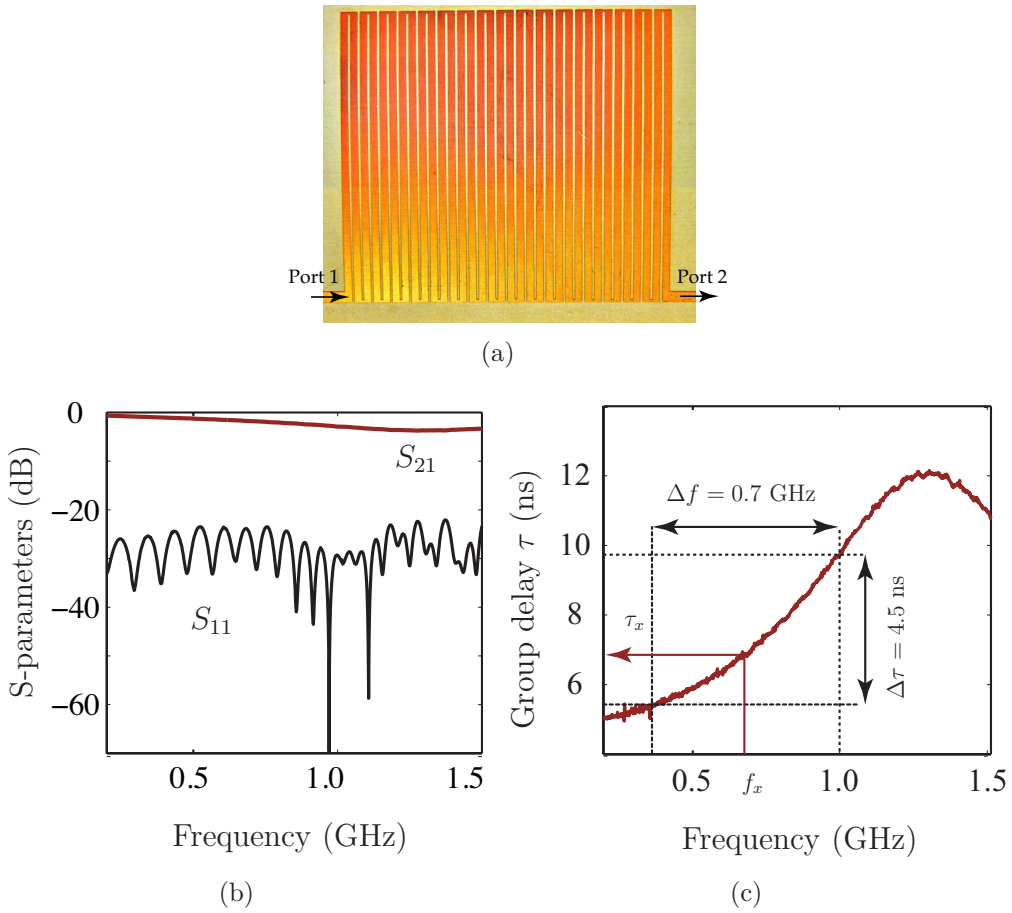

Figure 3.3 Microstrip C-section all-pass network used as the dispersive delay line in the system shown in Fig. 3.2(a). a) Photograph of the C-section structure. b) Measured S-parameters and c) Group delay $\tau(\omega)$.

3.3.2 Loop System Implementation

The complete system prototype is shown in Fig. 3.4(a) while its schematic, showing the various components along with the biasing networks and capacitors for DC and low-frequency isolation, is represented in Fig. 3.4(b). The corresponding experimental setup is shown in Fig. 3.4(c). The prototype consists of an RF mixer (ADE-42MH from Minicircuits) which modulates a time-domain Gaussian pulse (with fixed width in all forthcoming experiments), generated by an arbitrary pulse generator, with an input signal f_{LO}. This produces the modulated input pulse $v_{\mathrm{in}}(t)$ which is injected into the loop. An attenuator (PAT from Minicircuits

with 50 Ω input and output impedance) is placed just before the mixer as a precaution to minimize any reflection that may occur in case the input impedance of the RF mixer deviates from 50 Ω. Another attenuator (3-dB) is placed at the output of the mixer to reduce signal transmission toward the input port through the mixer due to possible mismatch in the loop circuit. The signal $v_{\text{in}}(t)$ enters the loop and passes through the DDS. The DDS output is then amplified by using an MMIC amplifier (ERA-5 from Minicircuits) to compensate for the loss experienced by the signal. A part of this amplified signal is extracted using a power divider (ADP-2-10 from Minicircuits), which is fed to an oscilloscope for monitoring the signal in the loop for each turn. The rest of the amplified signal is maintained in the loop and passed through a coaxial cable (external to the board here) exhibiting a constant group delay τ_0 (non-dispersive). The delayed signal passes then through another attenuator (3 dB) in the loop. This attenuator acts as an isolation device between the junction impedance Z_1 (ideally 25 Ω) and $Z_2 = 50$ Ω, as indicated in the schematic of Fig. 3.4(b). The attenuators were used here as a simple and low-cost solution for handling mismatches in the proof-of-concept prototype. A straightforward higher-performance but higher-cost approach would be to replace the attenuators by an isolator (with 50 Ω input and high output impedance) placed after the mixer to achieve $Z_1 = 50$ Ω.

3.3.3 Calibration

Before operation, the loop system must be calibrated to account for the effect of multiple turns and for the effect of the delay τ_0 induced by the non-dispersive delay line and the other loop elements. The calibration consists essentially in determining τ_0, which may take different values corresponding to different cable lengths or electronically tuned electric loop lengths for the measurement or processing of different signals. In a fixed loop system, for instance integrated on a chip and accomplishing a pre-determined function, τ_0 would be invariable and could therefore be predetermined at the circuit design stage, so that the calibration presented here could be skipped.

In order to perform calibration, a modulated pulse $v_{in}(t) = v_0(t)\sin(\omega_x t)$, with a known modulation frequency ω_x within the range of the used DDS, is injected into the system. The corresponding output signal $v_{out}(t)$, measured by an oscilloscope, is shown in Fig. 3.5 for a typical modulated signal. According to (3.1), the time difference between $n_x + 1$ peak maxima in $v_{out}(t)$ is

$$\Delta\tau_{x,n} = n_x\tau_x + (n_x - 1)\tau_0, \tag{3.3}$$

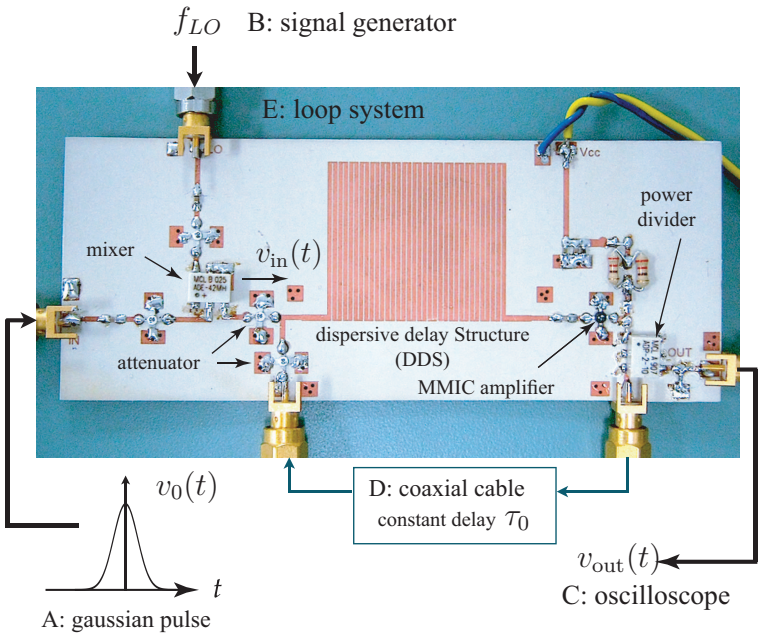

(a)

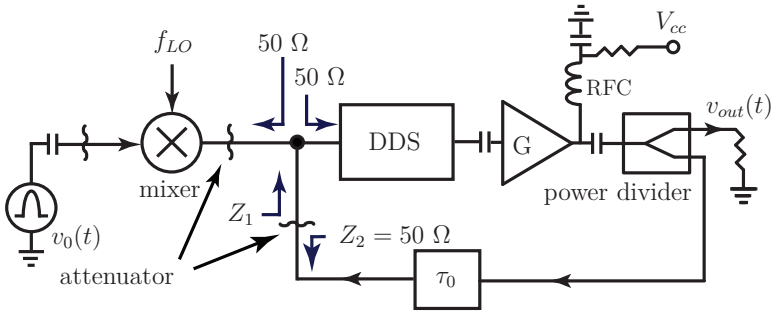

(b)

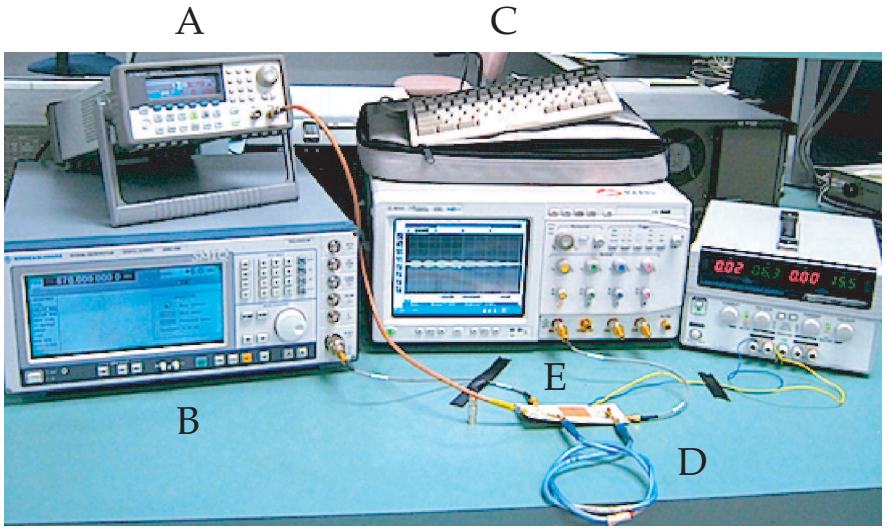

(c)

Figure 3.4 Experiments. a) System prototype, corresponding to Fig. 3.2(a), and incorporating the DDS of Fig. 3.3. b) Schematic. c) experimental setup, with corresponding A, B, C, D and E labels between (a) and (b). Only the major components are indicated.

where $\tau_x = \tau(\omega_x)$ and $\Delta\tau_{x,n} = \Delta\tau_n(\omega_x) = \tau_{n+k}(\omega_x) - \tau_k(\omega_x)$, k being an arbitrary integer and n_x being chosen large enough to allow accurate time resolution. From this equation, we obtain

$$\tau_0 = \frac{\Delta\tau_{x,n} - n_x\tau_x}{n_x - 1}. \tag{3.4}$$

Since τ_x is available from the known group delay response of the DDS, which is given in Fig. 3.3(c) in the case of the presently considered C-section DDS, the terms of this expression are all determined. Therefore, τ_0, which is a constant under the assumption that the elements of the loop other than the DDS exhibit negligible dispersion within the operation bandwidth, has been determined. This completes the calibration procedure. The calibration data for the signal in Fig. 3.5 are given in the caption of the same figure.

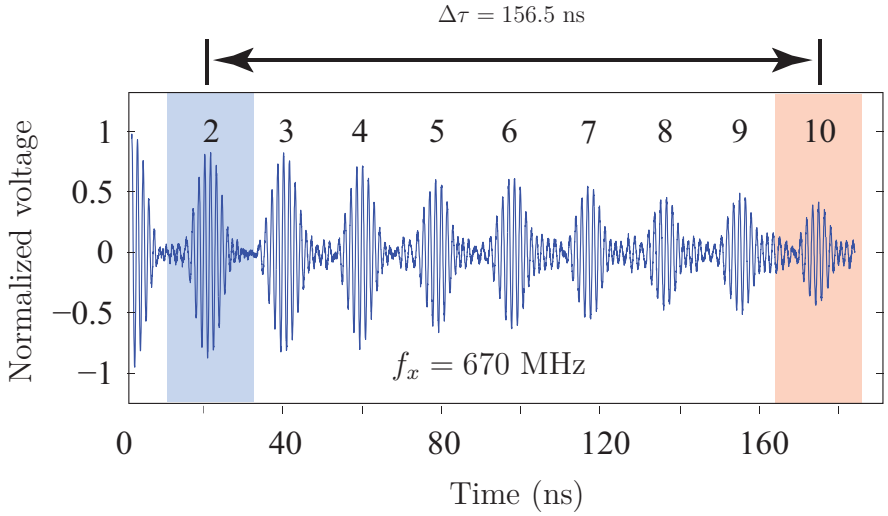

Figure 3.5 Calibration (measured) time-domain output signal $[v_{out}(t)]$ for an input pulse $[v_{in}(t)]$ modulated by a known frequency ω_x using the circuit prototype and experimental setup of Fig. 3.4. The results used here in connection with (3.4) are $f_x = 670$ GHz, corresponding according to Fig. 3.3(c) (or a more accurate DDS loop-up table) to $\tau(\omega_x) = 6.95$ ns, and $n = 8$ with $k = 2$, leading to $\tau_0 = 14.42$ ns.

3.3.4 Frequency Meter Application and Results

The frequency meter application is straightforward once τ_0 had been determined following the calibration procedure described in the previous section.

This time, the center (or modulation) frequency of the input signal $v_{in}(t)$ is unknown and must be determined by the loop system. The time difference $\Delta\tau_n$ between $n+1$ peak maxima

of the output signal $v_{out}(t)$ is measured, where n is chosen large enough to provide the desired time-frequency resolution. This time difference has the same form as that obtained in the calibration procedure [(3.3)] and reads

$$\Delta\tau_n = n\tau(\omega) + (n-1)\tau_0, \tag{3.5}$$

where τ_0 has been determined in (3.4). The delay incurred to the signal for a single pass across the DDS is obtained by inverting this relation, i.e.

$$\tau(\omega) = \frac{\Delta\tau_n - (n-1)\tau_0}{n}. \tag{3.6}$$

From this point, the unknown frequency is found by consulting the look-up table associated with the DDS, corresponding to Fig. 3.3(c) in the presently considered case of a C-section DDS.

An experimental demonstration of the frequency meter application is provided in Fig. 3.6 with numerical results in the caption of the same figure. The test frequency (f_1 or f_2), which is supposed to be unknown and is to be determined in a practical scenario, is assigned to f_{LO} by the generator. This frequency is determined by (3.6) with the delay-frequency mapping of Fig. 3.3(c) by measuring a delay $\Delta\tau_n$ at a selected turn number n with respect to a reference turn number k. Figure 3.6 demonstrates a frequency resolution of at least 219 MHz resolution, corresponding to the testing frequencies difference $f_2 - f_1$ for a turns difference if $n = 10 - 2 = 8$, which is considered sufficient as a proof of concept. However, it is to be noted that this resolution can be increased by increasing the number of turns.

The effective (system) group delay response $\tau_n(\omega)$ constructed from experimental frequency sample measurements similar to those of Fig. 3.6 is shown in Fig. 3.7 by circle markers. This graph also plots in continuous curves the responses corresponding to n times the group delay of the non-looped DDS, $n \times \tau(\omega)$. Good agreement is observed between the two types of results. The slight observed discrepancies are due to small uncertainty in the sampling points at the peak maxima. Such discrepancies are reduced for increasing values of n, as may be seen by comparing the curves for $n = 4$ and $n = 8$, which is the very principle of the proposed loop resolution enhancement. This graph clearly demonstrates the n-fold $\Delta\tau \times \Delta f$ product enhancement achieved by the proposed loop system.

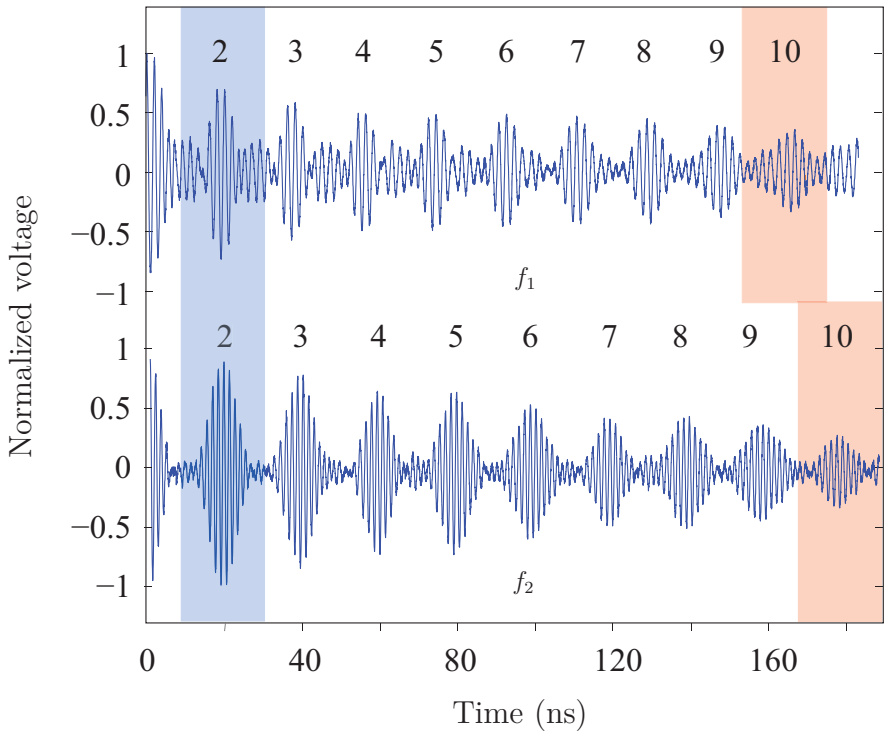

Figure 3.6 Measured time-domain output signals $[v_{out}(t)]$ for input gaussian pulses $[v_{in}(t)]$ pulses modulated by two different frequencies using the circuit prototype and experimental setup of Fig. 3.4. Using the calibration of Fig. 3.5 ($\tau_0 = 14.42$ ns), the two unknown frequencies, f_1 and f_2 are accurately determined by (3.6) for $n = 8$ with Fig. 3.3(c), leading to the results $f_1 = 484$ MHz from the measured delay of $\Delta\tau_8 = 151.89$ ns and $f_2 = 703$ MHz from the measured delay of $\Delta\tau_8 = 157.31$ ns, which correspond to the test frequencies imposed by the generator.

3.3.5 Frequency Discriminator Application and Results

A frequency meter is a useful device in its own rights for instrumentation, where it allows the accurate measurement of continuous signals. However, the more sophisticated operation of frequency discrimination is of even higher interest in broadcast and communication applications. For instance, frequency discriminators are of paramount importance in FM radio for the demodulation of frequency modulated signals. Moreover, in adaptive wireless networks, they may be used to identify free frequency bands and henceforth increase the channel spectral efficiency.

The proposed loop system can be readily used also as a frequency discriminator. In this case, the only difference is the simultaneous presence of several unknown frequencies in the input signal, whereas the frequency meter application demonstrated in the previous section considered single modulation frequency signals. However, the frequency extraction procedure

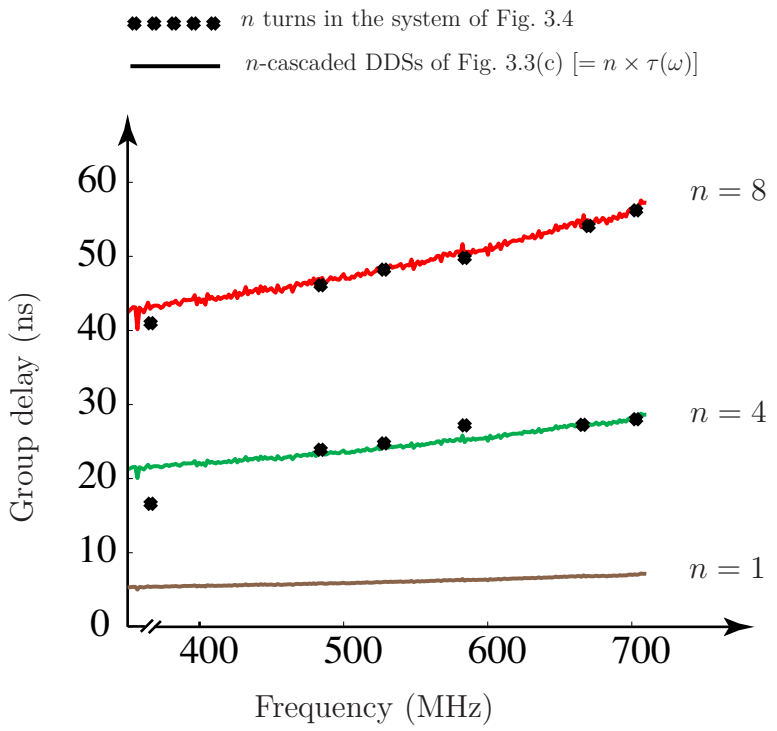

Figure 3.7 Measured effective group delay versus frequency (markers) for different number of turns in the system of Fig. 3.4. For comparison, the curves corresponding to $n \times \tau(\omega)$, where $\tau(\omega)$ is the group delay of a single C-section all-pass network in Fig. 3.3 (no loop), are also shown (solid lines).

for each of these frequencies, once the pulse have been separated in time, is exactly the same as in the frequency meter application. This operation of frequency discrimination corresponds to the illustration of Fig. 3.2(b).

An additional difficulty in the frequency discriminator is the necessity to avoid overlap between the resolved pulses. This may be solved by using an electrically longer non-dispersive delay line, so as to increase τ_0 and thereby the time spacing between the repeated pulses in the output signal. The demonstration of frequency discrimination for the two chosen input frequencies 333 MHz and 782 MHz, using a longer cable for proper discrimination, is presented in Fig. 3.8. This corresponds to a frequency resolution of 449 MHz after a turn difference of $n = 6 - 1 = 5$. As for the frequency meter application, this resolution can be enhanced by increasing the number of turns.

It should be noted that the measured results of Fig. 3.6 and 3.8 for the proof-of-concept prototype demonstrated in this section, do not show any oscillation, indicating that the loop is stable.

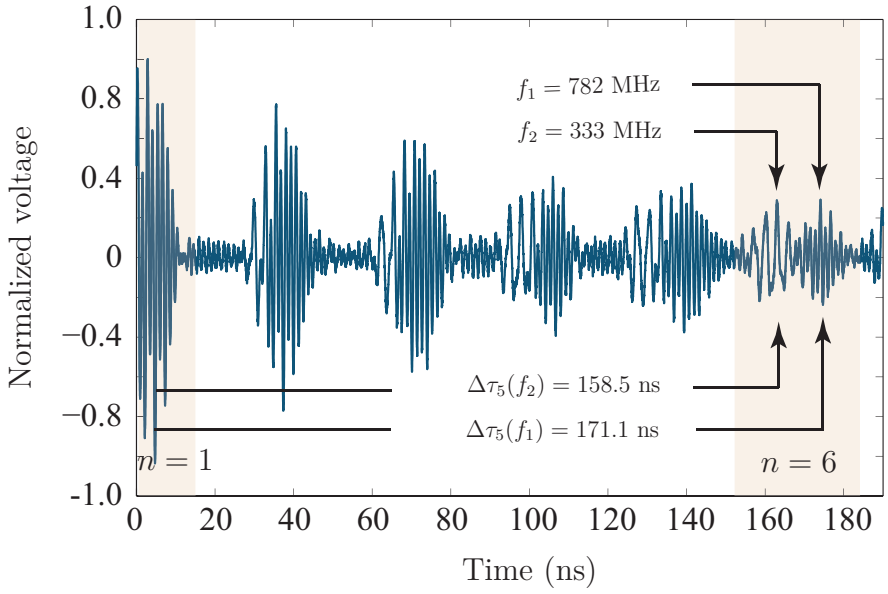

Figure 3.8 Measured time-domain output signal [$v_{out}(t)$] for an input gaussian pulse, $v_0(t)$, modulated by a two tone signal in the system prototype of Fig. 3.4(a), demonstrating the concept of frequency discrimination. Here, τ_0 has been increased from 14.42 ns to 33.13 ns, compared to its value in the application of the frequency meter demonstrated in Fig. 3.6, in order to avoid pulse overlap.

3.4 Possible Improvements

Although the results of Figs. 3.6 to 3.8 well demonstrate the proof-of-concept of resolution enhancement from increased group delay slope in the proposed loop system, and the specific applications of a frequency meter (Fig. 3.6) and a frequency discriminator (Fig. 3.8), several improvements are possible in the circuit implementation of Fig. 3.4(a).

Firstly, in the simple loop configuration of Fig. 3.2, the time-domain width of the pulse progressively increases due to dispersion as the number of turns increases, which would ultimately lead to an unavoidable self-overlap. This effect, while useful and essential in applications such as real-time Fourier transformers, is undesired in other applications, such as frequency meters and frequency discriminators, for instance, where time spreading limits the time resolution achievable by the system. In such cases, a more sophisticated design may be envisioned, where a pulse reshaping and amplifying device such as a Schmitt trigger [48] would be incorporated in the loop to eliminate the problem of spreading, at the expense of additional complexity related to the required frequency conversion for base-band operation of the trigger. In this manner, a perfect $n\times$ resolution enhanced system can be theoretically realized, although cumulated time drifts would impose practical limitations to the system.

Secondly, in the present implementation of the loop system, the commensurate C-section network used as the DDS exhibits a microstrip-type frequency increasing dielectric and conductor losses, where losses scale with frequency in the former case and with the square root of frequency in the latter case. This well-known effect is clearly visible in the decreasing amplitude transmittance plotted in Fig. 3.3(b). This effect restricts the upper limit of the operation frequency of the system, where the difference between the amplitude of the high and low frequency components constantly increases with the number of turns, eventually leading to severe distortions in the signal. This effect can be mitigated by using a high quality substrate with the lowest possible losses, such as alumina, or even air membrane suspended structures, to achieve a transmittance as flat as possible across the frequency band of operation.

Finally, the performance of the overall circuit can be considerably improved by using components of larger bandwidth and higher performance, especially the mixer (also with higher LO-RF rejection) and the amplifier. Moreover, the group delay of the various components (except the DDS) should ideally exhibit a constant group delay response across the entire operation bandwidth. It should be noted that the power divider, currently used in the demonstrated circuit (Fig. 3.4(a)) to sample the signal after each turns, also suffer of limited bandwidth. However, this component is not essential in the system and may be replaced by a simple switch associated with a counter, which would be closed to the output path after the number of turns corresponding to the desired group delay slope has been accomplished.

3.5 Conclusions

A novel increased group delay slope loop scheme has been proposed to enhance the time-frequency resolution of dispersive delay structure (DDS) components for microwave analog signal processing systems. This scheme has been experimentally demonstrated in a frequency meter and in a frequency discriminator.

The proposed resolution enhancement system provides a solution to the unpractical approach of cascading DDS units, which would lead to excessively large device footprint, unacceptably high insertion loss and severe signal-to-noise reduction. In addition to frequency meters and frequency discriminators, it may readily by applied to various other real-time systems, such as real-time Fourier transformers, convolvers, correlators and compressive radars.

CHAPTER 4 ARTICLE 2: LOW-COST ANALOG PULSE COMPRESSION TECHNIQUE BASED ON MIXING WITH AN AUXILIARY PULSE

Babak Nikfal, Shulabh Gupta, and Christophe Caloz

IEEE Microw. Wireless Compon. Lett., vol. 22, no. 3, pp. 150-152, Mar. 2012.

A low-cost analog pulse compression technique is proposed and experimentally demonstrated for a quasi-gaussian pulse. This technique consists in multiplying the pulse to compress with an auxiliary baseband gaussian pulse, which results in a compression of $\sqrt{2}$, and re-injecting this pulse n times around a loop including an amplifier, a delay line and an isolator, so as to achieve a compression factor of $\sqrt{1+n}$. In the experiment, a pulse width compression by a factor of 2.85 is achieved after the 9^{th} turn, in good agreement with the theory. Due to its inherent analog nature, the proposed system is flexible, easy to implement, frequency scalable and capable to handle ultra-wideband (UWB) signals.

4.1 Introduction

Pulse compression techniques are important tools for the generation of ultra-wideband (UWB) microwave signals, as they offer strong immunity to interferences, high energy efficiency and low transmitter complexity. For example, in compressive radars, the target resolution is inversely proportional to the pulse width [35, 49]. UWB pulses also find applications in impulse radio communications [49] and medical imaging [50].

Conventional compression pulse techniques are of two types: digital and analog. The digital techniques are most often based on fast Fourier transforms (FFTs) and matched filters [51] [52]. They require fast digital processors, which may be very complex in the case of large pulse bandwidth, prohibitively expensive at millimeter-wave frequencies, and suffering from high power consumption. The analog techniques are primarily based on dispersive delay structures (DDSs). In these techniques, the pulse to compress is mixed with a chirped signal, which results in a chirped modulated pulse. This pulse is injected into a DDS with the opposite delay-frequency response, so as to produce the compressed pulse [53]. Although conceptually simple, this techniques suffers from major drawbacks. First, it requires a fast and broadband chirp generator, consisting of a tunable oscillator and a voltage ramp generator (i.e., voltage controlled oscillator or VCO), which is both expensive and difficult to implement. Secondly, it requires a DDS, implemented for instance in surface acoustic wave (SAW) technology [12] or in chirped microstrip technology [53], which are too lossy for pulse compression at

microwaves. Unfortunately, photonics DDSs [54], which can be very efficient, do not have direct counterparts at microwaves.

We propose here a novel low-cost analog pulse compression technique based on mixing with an auxiliary pulse. Due to its analog nature, the proposed technique is inherently wideband and scalable to high frequencies. Moreover, it features higher efficiency and low cost as compared to DDS-based conventional microwave analog pulse compression techniques.

4.2 Proposed Pulse Compressor System

4.2.1 Principle

Consider a modulated gaussian pulse of full-width half maximum (FWHM) T_0, $v_{\text{in}}(t) = \exp(-At^2/T_0^2)\sin(2\pi f_{LO}t)$, where $A = 4\ln 2$, as shown in Fig. 4.1(a). The objective is to compress this pulse into a new pulse with smaller FWHM, i.e., $T_{\text{out}} < T_0$. $v_{\text{in}}(t)$ may be generated by mixing the baseband gaussian pulse $v_0(t)$ with a continuous wave signal of frequency f_{L0}, as illustrated in the upper left part of Fig. 4.1(a). The fundamental principle of the proposed technique is depicted in Fig. 4.1(a). The modulated input pulse $v_{\text{in}}(t)$ is multiplied with an auxiliary baseband gaussian signal of equal pulse duration (T_0), $v_{\text{aux}}(t)$, which produces the output signal $v_{\text{out}}(t) = \exp[-A(t/T_0)^2]\exp[-A(t/T_0)^2]\sin(2\pi f_{LO}t)$, which can be written as

$$v_{\text{out}}(t) = \exp\left[-A\left(\frac{t}{T_{\text{out}}}\right)^2\right]\sin(2\pi f_{LO}t), \tag{4.1}$$

where $T_{\text{out}} = T_0/\sqrt{2}$. Thus, the FWHM of the original signal has been compressed by a factor $\sqrt{2}$ in the multiplication process.

Higher compression may be achieved from this compression principle by repeating the multiplication process in a cascaded-network system. In such a system, the compressed pulse $v_{\text{out}}(t)$ at the output of Fig. 4.1(a), which may be renamed $v_{\text{out},1}(t)$, would be further multiplied with a baseband pulse of the same width (T_0), yielding a narrower signal, of width $T_0/\sqrt{3}$. This new signal, which may be called $v_{\text{out},2}(t)$, would then be multiplied again with the same baseband pulse, yielding a pulse $v_{\text{out},3}(t)$, of even narrower width, $T_0/\sqrt{4} = T/2$, and so on. After n successive multiplications, the signal would be $v_{\text{out},n}(t) = \exp[-A(t/T_0)^2 t]^n \exp[-A(t/T_0)^2\sin(2\pi f_{LO}t)$ i.e,

$$v_{\text{out},n}(t) = \exp\left[-A\left(\frac{t}{T_0/\sqrt{n+1}}\right)^2\right]\sin(2\pi f_{LO}t). \tag{4.2}$$

Thus, the FWHM has become $T_{\text{out},n} = T_0/\sqrt{n+1}$, which represents a compression factor of $\sqrt{n+1}$.

A much more cost-effective and compact alternative to such a cascaded-network architecture is the feedback-loop system depicted in Fig. 4.1(b). This system requires indeed only two mixers and one amplifier, as opposed to $n+1$ mixers and n amplifiers in the cascaded-network case, plus one power splitter, a delay line and an isolator. It operates as follows. A single modulated pulse $v_{\text{in}}(t)$, typically obtained by mixing $v_0(t)$ with a continuous wave of frequency f_{LO} using mixer #1, is multiplied with a baseband pulse $v_{\text{aux}}(t)$ using mixer #2. In accordance with (4.1), $v_{\text{in}}(t)$ gets compressed by a factor $\sqrt{2}$, resulting in a new pulse, $v_{\text{out, 1}}(t)$, within the loop. This compressed pulse is divided into two parts using a power splitter. One part represents the output of the system, $v_{\text{out}}(t)$, and is used to monitor the signal circulating around the loop. The second part is delayed by an amount τ, amplified by a factor G and fed back into mixer #2, where it is again multiplied, with a new incoming baseband gaussian pulse. This generates a modulated pulse, $v_{\text{out, 2}}(t)$, with an even smaller pulse width which is sent in turn around the loop. This process is repeated several times, injecting a new baseband pulse into mixer #2 every time a modulated pulse reaches this mixer from the loop. Consequently, in accordance with (4.2), after n turns around the loop, the overall pulse width $T_{\text{out},n}$, of $v_{\text{out, n}}(t)$ has reduced $T_0/\sqrt{n+1}$, corresponding to a compression factor of $\sqrt{n+1}$.

Note that this compression scheme requires $v_{\text{aux}}(t)$ to be a periodic baseband gaussian pulse signal of period T, chosen such that the compressed modulated pulse which is being fed back from the loop into mixer #2 is synchronized with the next incoming baseband gaussian pulse. This requires a delay of $\tau = T$, assuming ideal components with zero group delay. The delay element avoids overlap between the trailing and leading parts of the pulse traveling around the loop. The amplifier is obviously used to compensate for the various losses incurred along the loop. In addition, an isolator is placed along the loop to ensure proper matching at the junction between the two mixers. In an actual system, the isolator might be implemented by transistor circuit [55] or may be replaced by matching networks [2].

4.2.2 Features and Benefits

The proposed pulse compressing technique offers several benefits as compared to the conventional techniques. Firstly, it is completely analog in nature and therefore, when compared to digital techniques, it provides larger bandwidth and scalability to higher frequencies. Secondly, the proposed system does not require a chirp generator, in contrast to a DDS-based system, which dramatically reduces the cost of the system. Thirdly, in the loop architecture,

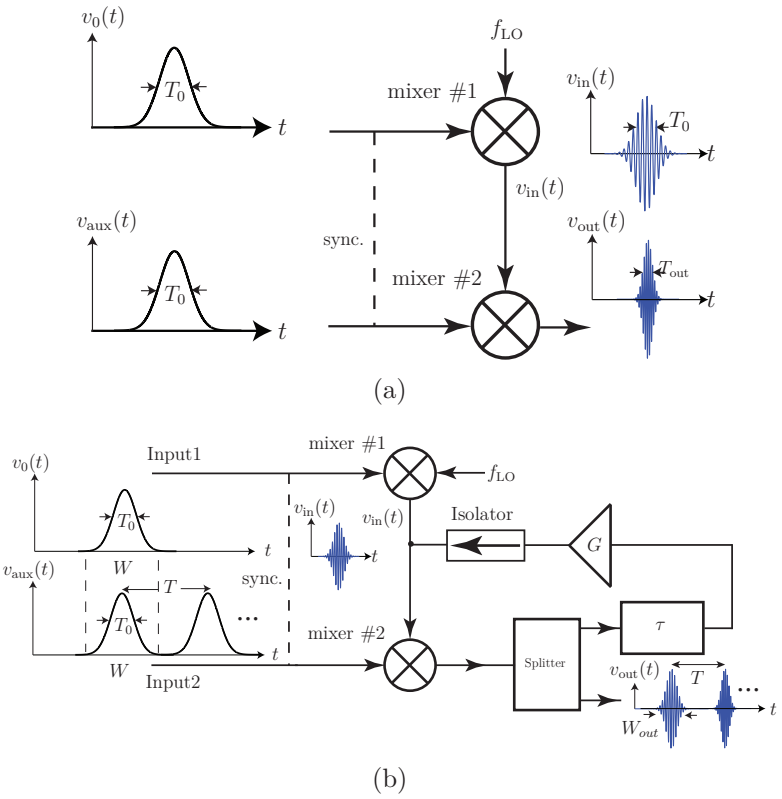

Figure 4.1 Proposed pulse compressor based on mixing with an auxiliary modulated pulse. (a) Simplest system, compressing the signal according to (4.1). (b) Loop-enhanced system, compressing the signal according to (4.2).

the modulated pulse propagating along the loop is regenerated and amplified at each turn, which maintains a high signal-to-noise ratio (SNR) in the system. Moreover, since the signal is amplified at each loop turn, a low gain amplifier is sufficient to compensate for the losses of the components in the loop, in contrast to case of a DDS-based system where a high gain amplifier is required to compensate for the high loss of the DDS. Furthermore, the system can be improved by replacing the power splitter with a time-gating mechanism using a switch in order to select out of the system only the desired n^{th} pulse, corresponding to the desired $\sqrt{n+1}$ compression factor. Table 4.1 compares the proposed pulse compression technique with conventional techniques. It is to be noted that although the pulse compressing scheme has been presented here specifically for gaussian pulses, it is applicable for wide range of practical pulses, which are typically close to gaussian pulses, as will be shown in the system demonstrated in Sec. 6.4.

4.3 Experimental Demonstration

Fig. 4.2 shows a proof-of-concept setup for the proposed pulse compression scheme, corresponding to Fig. 4.1(b). A single modulated pulse $v_{\text{in}}(t)$ is injected into the loop and is mixed with a baseband quasi-gaussian pulse $v_0(t)$ of width $W = 10.76$ ns and 300 mV peak amplitude using mixer #2, resulting in a new signal, $v_{\text{out},1}(t)$. Due to the unavailability of a second gaussian pulse source, a rectangular pulse is used as $v_0(t)$, resulting in a modulated rectangular pulse $v_{\text{in}}(t)$ of amplitude 280 mVp-p. Consequently, after the first multiplication of $v_{\text{in}}(t)$ with $v_{\text{aux}}(t)$ at mixer #2, a modulated quasi-gaussian pulse of same duration as the baseband pulse, i.e., $W = 10.76$ ns is obtained, as shown in Fig. 4.3. It should be noted that this first multiplication does not contribute to pulse width compression. This signal represent $v_{\text{out},1}(t)$ with an amplitude of 65 mVpp after the splitter, as shown in Fig. 4.3. This is the signal that will circulate around the loop and that is to be compressed. Except for this difference, the operating principle of this experimental setup is exactly the same as in Fig. 4.1(b). The total loop delay, accounting for all the components in the loop, is 50 ns. The gain of the amplifier is 13 dB, while the power from the splitter (which may be avoided using the aforementioned time-gating/switch mechanism) drops by 6 dB, due to resistive loss of the component, and the insertion losses of the delay line and isolator combined is 3 dB. The rest of the loss is incurred by the mixer. Note that the total loop gain is always kept below unity in order to avoid satisfaction of the Barkhausen criterion for oscillation [56], thereby keeping the system stable at all times.

Table 4.1 Performance comparison with other techniques

technique	loss (dB)	BW (GHz)	ω_0 (GHz)	complexity
SAW (DDS) [12]	≈ 20	< 0.1	< 3	high (requires VCO)
chirped microstrip (DDS) [53]	≈ 10	high	high	high (requires VCO)
FFT [52]	≈ 0	< 0.1	<1	high
Proposed	≈ 7	high	high	low

The output signal is shown in Fig. 4.3(a). A gradual compression of the pulse width is clearly observed in this graph. The small variation which is observed in the pulse amplitude may be attributed to the frequency dependent transmission characteristics of the components in the loop ; this effect becomes increasingly important as the signal gets increasingly compressed, due to the related increased bandwidth.

As an example, comparing $v_{\text{out},9}(t)$ with $v_{\text{out},1}(t)$ in Fig. 4.3(b) gives a compression factor of

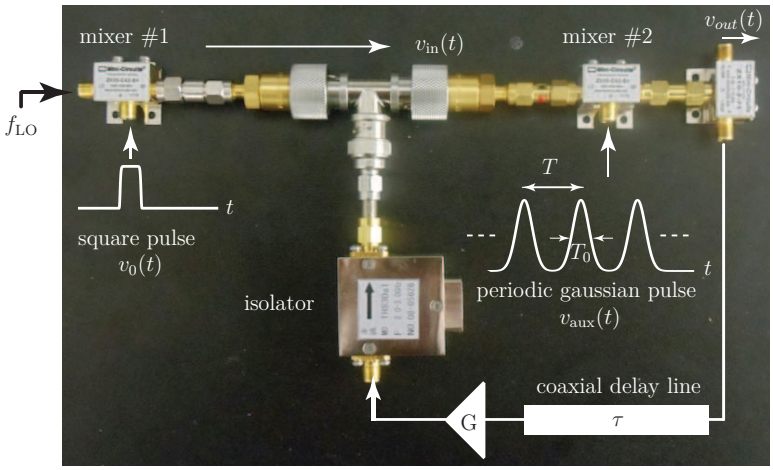

Figure 4.2 Pulse compressor setup based on the feedback architecture of Fig. 4.1(b), Delay line and Amplifier are the external components. The mixer and splitter models used are ZX-05-C42-S+ and ZX-10-2-71, respectively, both from Minicircuits. The isolator model is THS3Da1 (2-3 GHz).

$W_{\text{in}}/W_{\text{out}} = 10.76/3.77 = 2.85$, which is in close agreement with $T_{\text{out},n} = T_0/\sqrt{n}$ with $n = 9$, considering that the first multiplication does not contribute to the pulse width compression in the demonstration setup. The measured output is also compared with the analytical output, computed using (4.2), for the input square pulse. Good agreement between the output pulse widths is observed, with an error of 8%, which verifies the proposed pulse compression technique.

Further compression may be achieved, up to the point where the pulse bandwidth reaches the bandwidth of the loop, which is limited by the bandwidth of the different components along it. Thus, the maximal achievable compression of the system is limited by the bandwidth characteristics of the components along the loop. Moreover, the pulses eventually die out due to the less-than-unity gain of the loop required for stability.

4.4 Conclusions

A novel low-cost analog pulse compression technique based on mixing with an auxiliary pulse has been proposed and experimentally demonstrated for the case of a quasi-gaussian pulse. Using a feedback loop architecture, this system provides a compression factor of $\sqrt{n+1}$, after n^{th} turn around the loop. A pulse-width compression factor of 2.85 has been achieved in the experimental setup after the 9^{th} turn, as predicted. Due to its inherent analog nature, the proposed system is flexible, easy to implement, frequency scalable and capable of handling

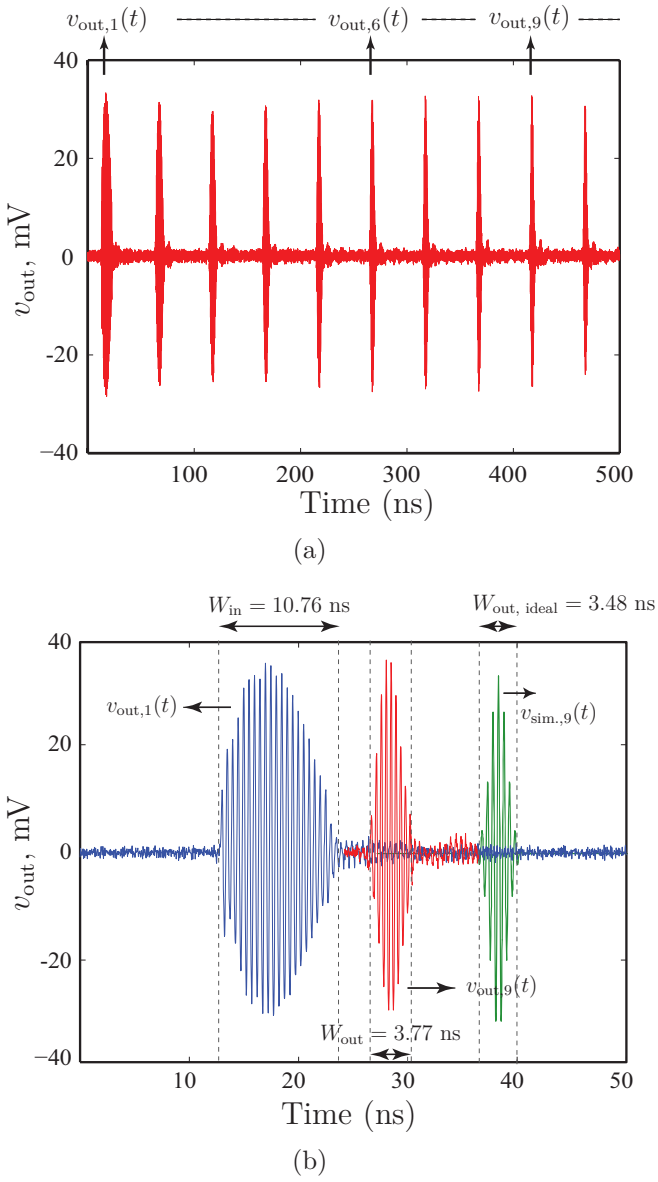

Figure 4.3 Experimental results for the compressor of Fig. 4.2. (a) Output signal $v_{\text{out}}(t)$. (b) Comparison of the first and the 9th output pulses showing an expected pulse width compression by a factor of 2.85. $f_{\text{LO}} = 2$ GHz. $v_{\text{sim.},9}(t)$ is simulated output using (4.2), which has been intentionally shifted by 10 ns for comparison, and $v_{\text{out},9}(t)$ is the measured output result.

UWB signals. It may find applications in compressive radar, impulse radio and medical imaging.

CHAPTER 5 ARTICLE 3: DISTORTION-LESS REAL-TIME SPECTRUM SNIFFING BASED ON A STEPPED GROUP-DELAY PHASER

Babak Nikfal, Daniel Badiere, Morris Repeta, Brad Deforge, Shulabh Gupta, and Christophe Caloz

IEEE Microw. Wireless Compon. Lett., vol. 22, no. 11, pp. 527-529, Nov. 2012.

The concept of real-time spectrum sniffing – featuring a simple and low-cost circuit architecture with straightforward frequency scalability – is introduced for cognitive radio systems. A stepped group-delay phaser is proposed and demonstrated to eliminate the issue of frequency resolution limitation due to the dispersion spreading induced by conventional phasers.

5.1 Introduction

The increasing demand for wireless connectivity within restricted radio frequency bands leads to interferences resulting in reduced data throughput and channel reliability in wireless networks. A potential approach to mitigate this issue is to analyze in real time the spectrum of the ambient signals so as to determine the available frequency bands and opportunistically use these bands for the signals to be sent. Such a spectrum analysis is typically performed by a *spectrum sniffer* [57] and plays a major role in cognitive radio systems [58]. Conventional spectrum sniffers are most often digital and based on the fast Fourier transform (FFT) techniques [59]. However, such sniffers require fast digital processors, which may be prohibitively complex and expensive for large bandwidths and high frequencies.

In this paper, we introduce the idea of *real-time* frequency sniffing, based on the real-time frequency discrimination [40, 60] enabled by dispersive delay structures with controllable group delay [2], called *phasers* [23]. Due to its passive nature and broadband nature of phasers, real-time spectrum sniffers are simple, broadband, fast and frequency scalable. In the case of conventional phasers, their frequency resolution is limited by pulse spreading. We propose here a stepped group-delay phaser scheme which eliminates this issue.

5.2 Real-time Spectrum Sniffer

5.2.1 Principle of Operation

Fig. 5.1 shows the principle of a real-time spectrum sniffer. The global signal in the environment of the sniffer, $v_{\text{in}}(t)$, which typically includes several communication channels, is picked

up by a broadband antenna and mixed with a baseband gaussian pulse $g(t)$ of duration T. This produces the multi-tone pulse $v_{\text{mix}}(t) = g(t)\sum_{n=1}^{N} c_n \sin(\omega_n t)$, where N is the number of frequency channels and c_n is either 1 or 0 depending on whether channel n is active or not. The signal $v_{\text{mix}}(t)$ is injected into the phaser, which temporally discriminates its different frequency components corresponding to the different channels, generating the signal $v_{\text{out}}(t) = \sum_{n=1}^{N} c_n v_n(t-\tau_n)$, where $\tau_n = \tau(\omega_n)$. This signal may then be envelope detected and amplitude reshaped using a Schmitt trigger with an appropriate threshold voltage v_{th}. As a result, a sequence of 1 and 0 bits is obtained, indicating the presence or absence of activity in the corresponding channels.

As seen in Fig. 5.1, discrimination between the channels occurs only if the separation between adjacent pulses, defined here as the distance between adjacent peaks, $\Delta\tau_{n,n+1}$, is larger than the durations of the related half pulses in $v_{\text{out}}(t)$, i.e.,

$$\Delta\tau_{n,n+1} > \frac{T'_n + T'_{n+1}}{2} = \Delta\tau^{\min}_{n,n+1}, \tag{5.1}$$

where T'_n is the duration of the n^{th} output pulse, with modulation frequency ω_n. Note that, due to the temporal dispersion typically induced by the phaser, and subsequent pulse spreading, $T'_n > T$, and therefore $\Delta\tau^{\min}_{n,n+1} > T$. This constraint limits the frequency resolution of the real-time spectrum sniffing, as we shall see next.

5.2.2 Pulse Spreading in Conventional Phasers

The effect of pulse spreading induced by dispersion in a *conventional phaser*, which we define here as a phaser with a non-zero group-delay slope over its entire bandwidth, is depicted in Fig. 5.2. An input modulated pulse of duration T and bandwidth B centered at the frequency ω_0 is injected into the phaser. While phasers may have different group delay responses, we consider here the case of a linear group delay for the sake of illustration, $\tau(\omega) = a\omega + b$, where a is the group-delay slope and b is a constant. Since the phaser assigns different delays to different spectral components, the input pulse spreads out in time, resulting in the broader output pulse with duration

$$T' = T + \Delta\tau = T + aB, \tag{5.2}$$

where the pulse broadening $\Delta\tau = aB$ corresponds to the group delay swing of the phaser over the bandwidth B of the signal. Equation (5.2) shows that the pulse broadening ($\Delta\tau$) is proportional to the group delay slope (a) of the phaser and to the bandwidth (B) of the signal ($\propto 1/T$).

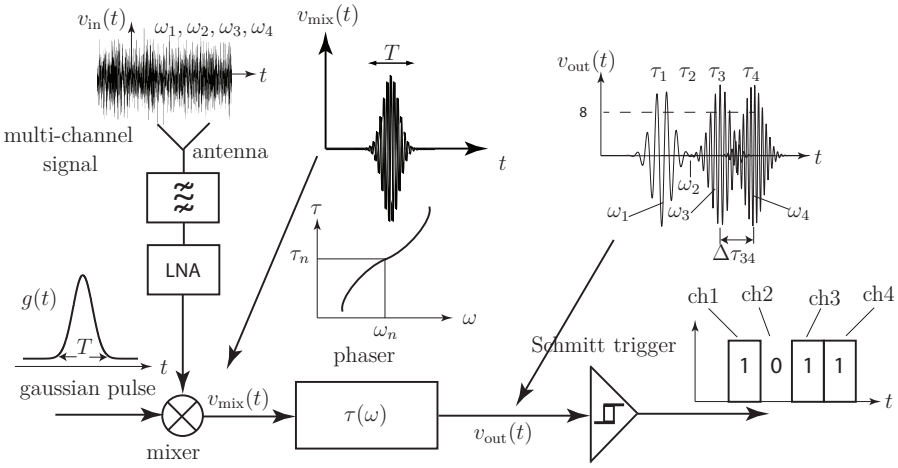

Figure 5.1 Principle of a real-time spectrum sniffer.

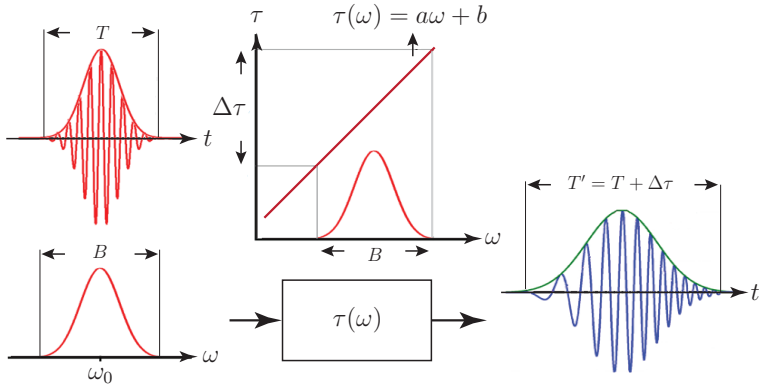

Figure 5.2 Pulse spreading due to dispersion in a conventional phaser. The figure shows the case of a phaser with a linear group delay, but the concept of pulse spreading holds for phasers with more complex responses.

5.2.3 Frequency Resolution Limitation due to Spreading

Consider a wireless environment with channels so close to each other that, with a given phaser (having for instance a linear group response as in Fig. 5.2), channel discrimination could not be achieved due to adjacent pulse overlapping in time (see Fig. 5.1). To solve this problem, one has to increase $\Delta\tau_{n,n+1} = \Delta\tau$ (equality for linear group delay) so as to satisfy (5.1). However, according to (5.2) where $\Delta\tau = aB$, this would require either increasing a or decreasing $T = 1/B$, which both would increase $T'_n = T'$ (equality for linear group delay), which defeats the initial purpose of satisfying (5.1). Thus, the spreading in a conventional phaser limits the frequency resolution $\Delta\omega = \omega_{n+1} - \omega_n$ of the sniffer, i.e., its capability to discriminate closely spaced channels in the environment.

5.3 Proposed Stepped Group-Delay Phaser

In order to suppress the frequency resolution limitation explained in Sec. 5.2, one should have a zero group-delay slope ($a = 0$) within each channel, so as to maintain there $T'_n = T$, and a non-zero group delay slope ($a \neq 0$) between the channels, so as to provide channel discrimination. This may be achieved by a stepped group-delay phaser, as shown in Fig. 5.3(a). With such a phaser, the slope of the group delay across the channel regions is zero, so that no spreading (and hence no distortion) occurs in these frequency ranges, while the channels are discriminated from each other by interposed non-zero group-delay slopes regions. This scheme leads to channel discrimination without pulse spreading, assuming that the bandwidth of $g(t)$ is confined within the channel bandwidth, all output pulses having the duration T as the input gaussian pulse, as illustrated in Fig. 5.3(b). Thus, the frequency resolution issue described in Sec. 5.2.3 has been eliminated. It should be noted that the frequency discrimination $\Delta\tau_{n,n+1} = \tau_{n+1} - \tau_n$ depends on the group delay slope of the phaser, which can be enhanced using several techniques such as a loop system [2].

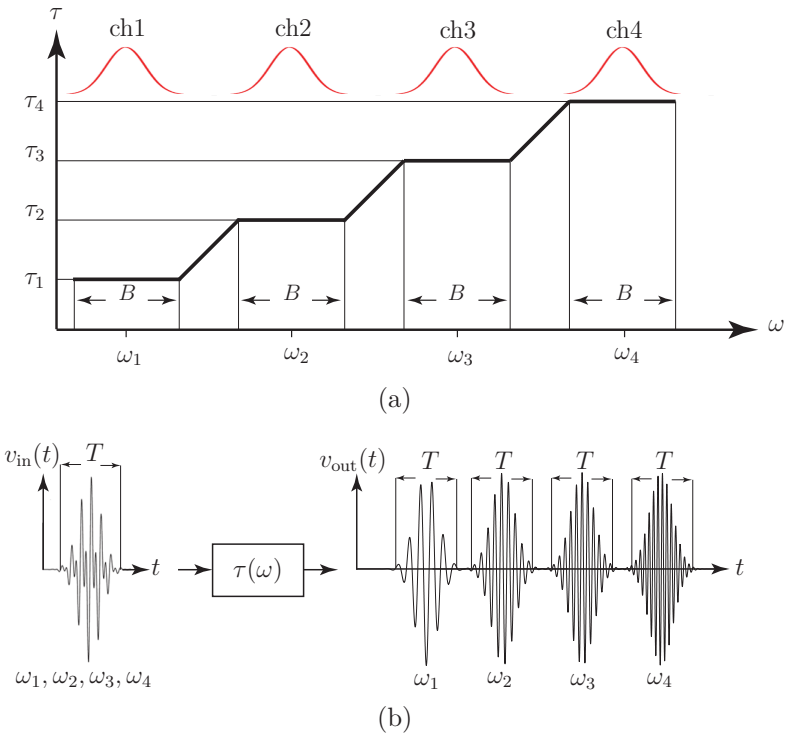

Figure 5.3 Proposed stepped group-delay phaser concept (case of $N = 4$ channels). (a) Group-delay versus frequency response. (b) Resulting distortion-less channel discrimination.

Phasers can be conveniently implemented using coupled transmission line all-pass structures, referred to as C-sections [3]. A C-section is formed by a four-port coupled-line network with interconnected through and isolation ports. By cascading several C-sections of different lengths and different coupling coefficients, so as to form a non-commensurate structure [3], a quasi-arbitrary group delay response can be synthesized, such as the stepped group delay response required in the proposed spectrum sniffer.

5.4 Experimental Demonstration

Let us consider the example of a four-channel short-range communication system (IEEE 802.11ad) with a total bandwidth of 9 GHz [61]. The group delay engineered non-commensurate C-section network required for spectrum sniffing in this application is implemented in stripline technology following the design procedure presented in [3]. Fig. 5.4 shows the measured S-parameters and group delay responses for a quasi-linear group-delay phaser and a stepped group delay phaser to be used next in two different frequency sniffers for comparison. The substrates used are Rogers 3602, with $\epsilon_r = 6.15$ and $\tan\delta = 0.0027$.

Large insertion loss, due to the large electrical sizes of the *unfolded* phaser structures, is observed in both cases. However, this is not prohibitive, considering the larger overall loss in competing digital spectrum sniffers. Moreover, dramatically lower loss may be achieved in waveguide phasers [7]. The insertion loss increases with frequency following the trend of dielectric and conductor losses. This non-uniformity may be overcome by resistive equalization [28]. A satisfactory group delay response is achieved in both designs.

Fig. 5.5 shows a proof-of-concept setup for the proposed frequency sniffer scheme. The combination of a multi-tone signal generator and three power combiners is used as the environment signal emulator. In this proof-of-concept design, the power levels of the input signals were adjusted to equalize the insertion loss non-uniformity of the phaser. A gaussian pulse of 2 ns was mixed with the multi-tone signal v_{in} to produce v_{out} at the output of the phaser after amplification.

Fig. 5.6 shows the measured output time-domain signals for the linear phaser of Fig. 5.4(a) [Fig. 5.6(a)] and the stepped phaser of Fig. 5.4(b) [Fig. 5.6(b)], respectively, when Channels 1, 3 and 4 are present and Channel 2 is absent. In the former case, the absence of signal in Channel 2 cannot be detected due to spreading, possibly leading to the erroneous deduction that the corresponding band is unavailable, whereas it clearly can in the latter case. Fig. 5.6(c) further shows the output of the stepped phaser when all the four channels are present, where the signals in all four channels are correctly identified.

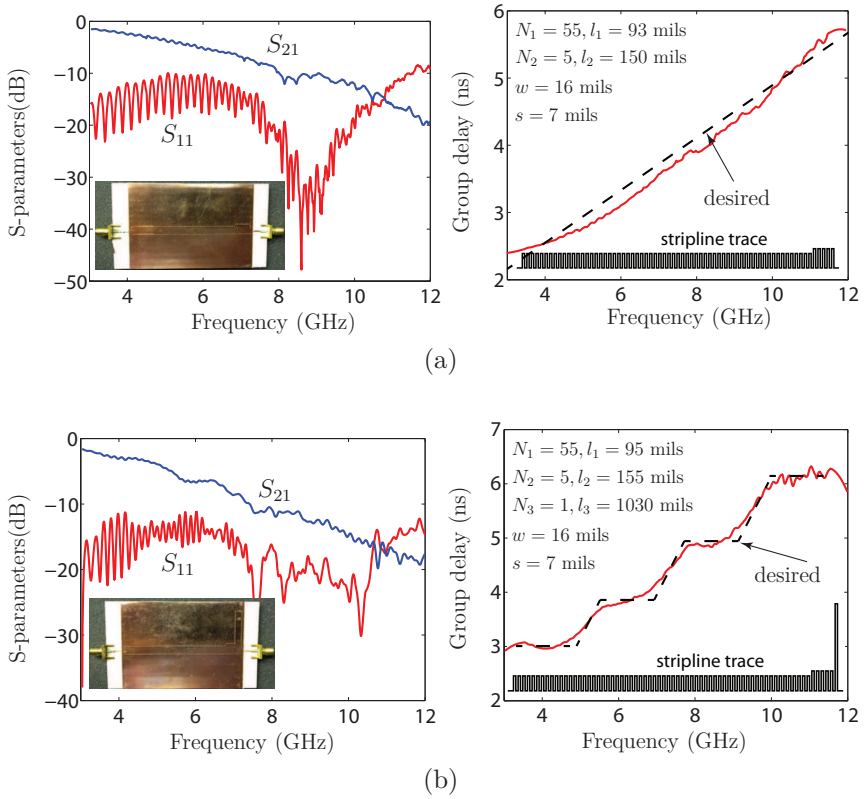

Figure 5.4 Measured responses for two different non-commensurate phasers in C-section stripline technology [3]. (a) Typical (quasi-linear) design, as in Fig. 5.2. (b) Proposed stepped group-delay design, as in Fig. 5.3. The design parameters – lengths ℓ_k of the N_k C-sections in each k^{th} group, strip widths (constant) w and strips spacings (constant) s – are indicated in the figures.

5.5 Conclusions

We have introduced the concept of real-time spectrum sniffing, featuring a simple and low-cost circuit architecture with straightforward frequency scalability. In order to suppress the frequency resolution limitation imposed by conventional phasers in such a system, we have proposed and demonstrated a stepped group-delay phaser. The resulting spectrum sniffer may find applications in cognitive radio systems.

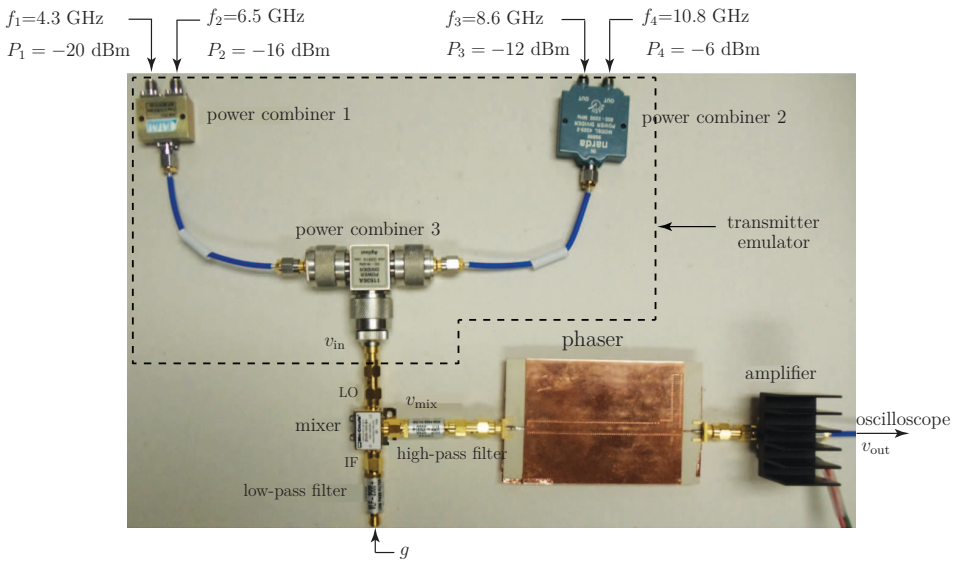

Figure 5.5 Proof-of-concept frequency sniffer setup based on the group-delay phaser of Fig. 5.4. The mixer and amplifier are Minicircuits ZX05-153+ and ZVA-213-S+. The filters are Minicircuits VLF2500+ and VHF3500+. The splitters are ATM P217, Narda 4325-2, and Agilent 11636A, respectively.

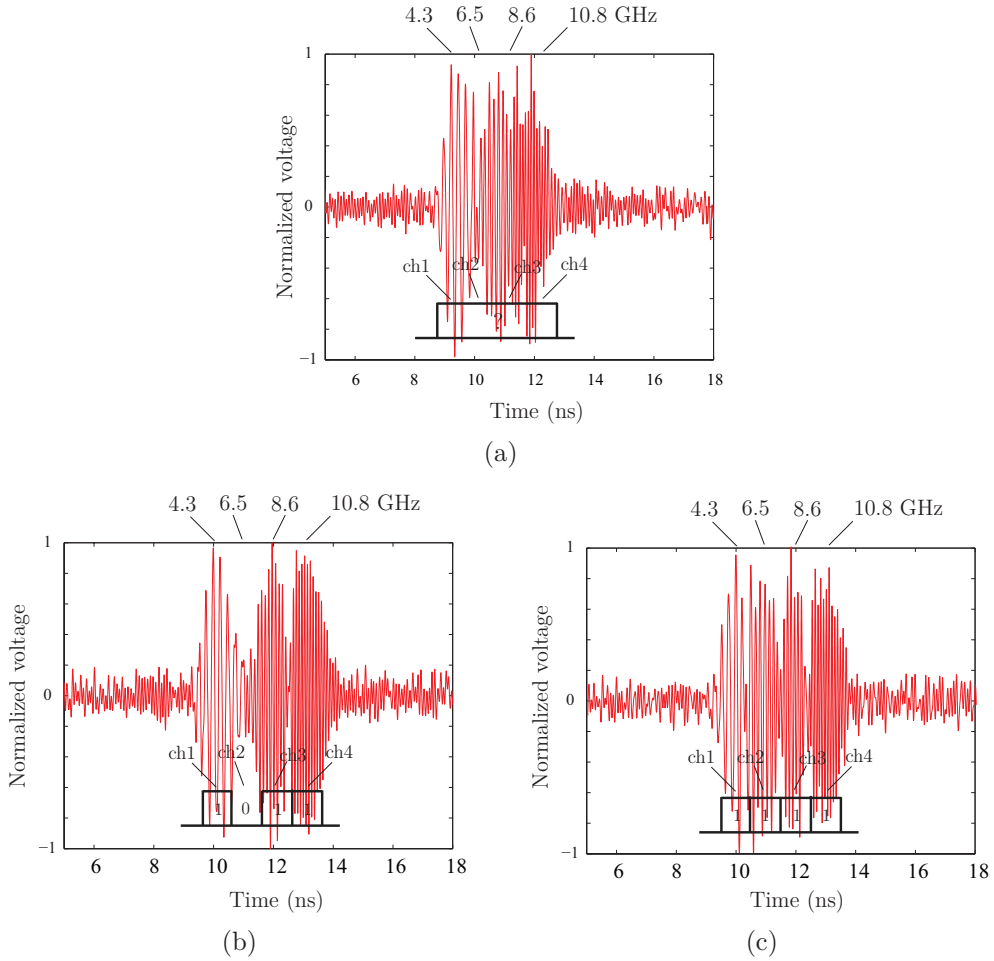

Figure 5.6 Measured signals of the output of the frequency sniffer of Fig. 5.5. for a input signal including in general the four channels centered at $f_1 = 4.3$ GHz, $f_2 = 6.5$ GHz, $f_3 = 8.6$ GHz, and $f_4 = 10.8$ GHz. (a) Linear phaser for channels 1, 3, and 4 ON and channel 2 OFF. (b) Stepped phaser for the same situation as (a). (b) Stepped phaser for channels 1, 3, and 4 ON and channel 2 OFF.

CHAPTER 6 ARTICLE 4: ENHANCED-SNR IMPULSE RADIO TRANSCEIVER BASED ON PHASERS

Babak Nikfal, Qingfeng Zhang, and Christophe Caloz

IEEE Microw. Wireless Compon. Lett., vol. 24, no. 11, pp. 778-780, Nov. 2014.

The concept of SNR enhancement in impulse radio transceivers based on phasers of opposite chirping slopes is introduced. It is shown that signal-to-noise ratio (SNR) enhancements by factors M^2 and M are achieved for burst noise and Gaussian noise, respectively, where M is the stretching factor of the phasers. An experimental demonstration is presented, using stripline cascaded C-section phasers, where SNR enhancements in agreement with theory are obtained. The proposed radio analog signal processing transceiver system is simple, low-cost and frequency scalable, and may therefore be suitable for broadband impulse radio ranging and communication applications.

6.1 Introduction

Impulse radio, a form of ultra-wide band signaling using pulse modulation, is a promising technology for high data rate communication networks with low complexity and low power consumption. It may for instance apply to wireless personal area networks, identification, positioning and wireless sensor networks [62–64]. However, impulse radio systems are particularly sensitive to noise and interferers since they are fundamentally amplitude modulation system. Increasing the power of the transmitted signal is not a solution for SNR enhancement, since it leads to increased power consumption, reduced system dynamic range due to the power amplifier, and exceeding of allowed power spectral density (PSD) limits.

To address this issue, we introduce here an enhanced-SNR impulse radio transceiver, based on the up-chirp and down-chirp dispersive delay structures with controllable group delay [2, 17, 65], called phasers [1,40]. Due to its passive and distributed nature and due to the broadband nature of phasers, the enhanced-SNR impulse radio transceiver is simple, broadband and frequency scalable.

6.2 Principle of the Transceiver

Figure 6.1 shows the principle of the proposed enhanced-SNR impulse radio transceiver. Figure 6.1(a) shows the block diagram of the transmitter. The message data, which are

reduced in the figure to a single baseband rectangular pulse representing a bit of information, is injected into the pulse shaper to be transformed into a smooth Gaussian-type pulse, $g(t)$, of duration T_0. This pulse is mixed with an LO signal of frequency ω_0, which yields the modulated pulse $v_{\text{Tx}}^{-}(t) = g(t)\cos(\omega_0 t)$, of peak power P_0. This modulated pulse is injected into a linear up-chirp phaser, and subsequently transforms into an up-chirped pulse, $v_{\text{Tx}}^{+}(t)$. Assuming energy conservation (lossless system), the duration of this pulse has increased to MT_0 while its peak power has decreased to P_0/M, where M is the stretching factor of the phaser, given by $M = T_{\text{out}}/T_0 = (T_0 + s\Delta\omega)/T_0$, where T_0 and T_{out} are the duration of the input and output pulses, respectively, s is the slope of the group delay response of the phaser (in s^2/rad), $\tau(\omega)$, and $\Delta\omega$ is the bandwidth of the pulse [5]. Finally, the up-chirped pulse $v_{\text{Tx}}^{+}(t)$ is boosted by a power amplifier and radiated by an antenna towards the receiver. Figure 6.1(b) shows the block diagram of the receiver. The incoming signal, $v_r(t)$, is picked up by the antenna, along with the noise of the channel, $v_n(t)$, which may consist of a superposition of Gaussian noise and burst noise. After bandpass filtering and low-noise amplification, the received up-chirped and noisy signal, $v_{Rx}^{-}(t)$, is injected into a linear down-chirp phaser. Alternatively, one may naturally use a down-chirp phaser in the transmitter and an up-chirp signal in the receiver. As a result, the instantaneous frequencies of the transmitted part of the signal are essentially equalized so as to compress the pulse to an enhanced waveform that is essentially identical to $v_{Tx}^{-}(t)$, whereas the burst noise is spread out in time, since it was not pre-chirped, and the Gaussian noise remains a Gaussian noise. So, the signal has been enhanced whereas the noise level has been either reduced (burst noise) or unaffected (Gaussian noise). Note that time expansion and associated peak power reduction in the transmitter also results in increased system dynamic range.

6.3 Signal-to-Noise Characterization

Let us now examine in more details how the signal is enhanced compared to noise and subsequently determine the SNR of the system. Figure 8.1 shows the powers of the signals in Fig. 6.1 that are relevant to this end.

First consider the scenario of a noise consisting only of burst noise, with the same carrier frequency and the same bandwidth as the signal. The signal to noise ratio at the input of the down-chirp phaser in the receiver is then

$$\text{SNR}_{\text{b}}^{-} = \frac{P_{\text{s}}^{-}}{P_{\text{b}}^{-}}, \tag{6.1}$$

where P_{s}^{-} is peak power of the up-chirped signal and P_{b}^{-} is the peak power of the burst

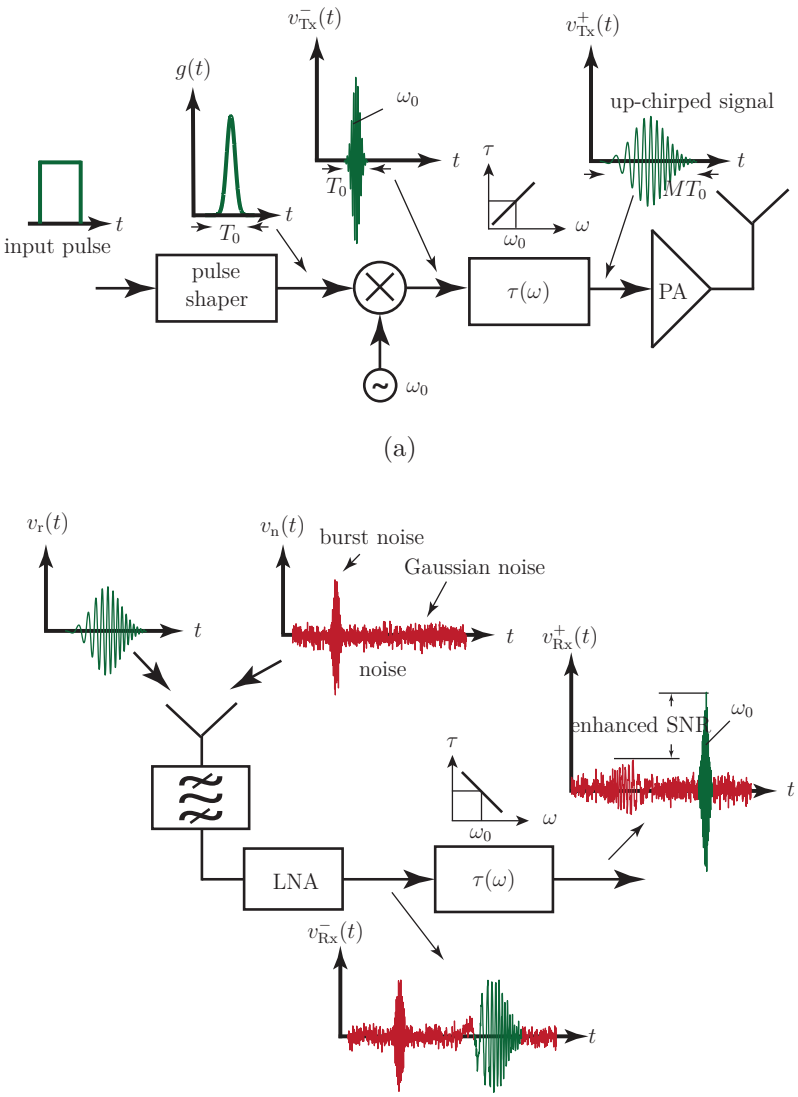

Figure 6.1 Principle of the proposed enhanced-SNR impulse radio transceiver. (a) Transmitter. (b) Receiver.

noise. As the signal passes through the phaser, its peak power reduces by a factor M due to time spreading and, consequently, the power at the output of the phaser is $P_{\mathrm{b}}^{+} = P_{\mathrm{b}}^{-}/M$. In contrast, the signal is enhanced by the factor M, due to dispersion compensation, so that the peak power at the output of the phaser is $P_{\mathrm{s}}^{+} = MP_{\mathrm{s}}^{-}$. As result, the output signal to burst noise ratio is

$$\mathrm{SNR}_{\mathrm{b}}^{+} = \frac{P_{\mathrm{s}}^{+}}{P_{\mathrm{b}}^{+}} = \frac{MP_{\mathrm{s}}^{-}}{P_{\mathrm{b}}^{-}/M} = M^2\,\frac{P_{\mathrm{s}}^{-}}{P_{\mathrm{b}}^{-}} = M^2\mathrm{SNR}_{\mathrm{b}}^{-}, \tag{6.2}$$

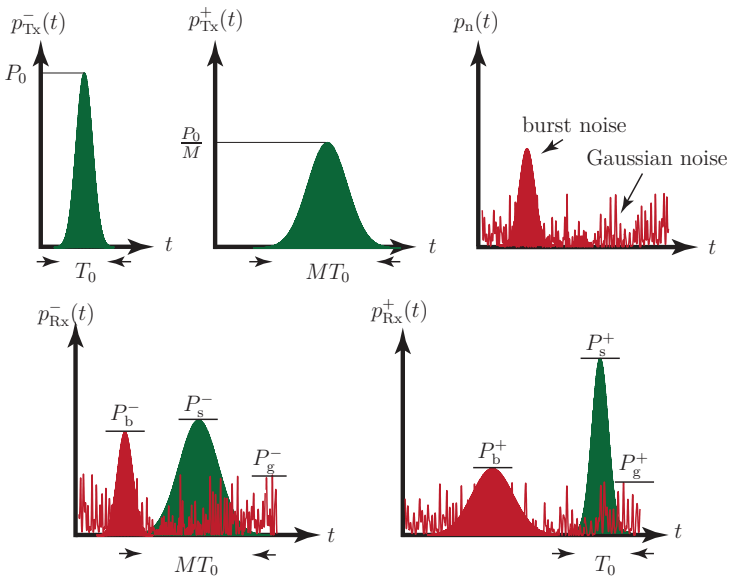

Figure 6.2 Powers of the signals in Fig. 6.1.

revealing that the burst noise has been enhanced by a factor M^2.

Consider now a second scenario, where the noise is a Gaussian noise only. The signal to noise ratio at the input of the down-chirp phaser in the receiver is then

$$\mathrm{SNR}^-_{\mathrm{g}} = \frac{P^-_{\mathrm{s}}}{P^-_{\mathrm{g}}}, \tag{6.3}$$

where P^-_{s} is again the peak power of the up-chirped signal and P^-_{g} is the peak power of the Gaussian noise. As in the previous scenario, the signal power is enhanced to $P^+_{\mathrm{s}} = MP^-_{\mathrm{s}}$. However, the power of the Gaussian noise does not change, i.e. $P^+_{\mathrm{g}} = P^-_{\mathrm{g}}$, since the effect of the phaser on such a noise is only to change its phase randomness. As a result, the signal to Gaussian noise ratio at the output of the phaser is

$$\mathrm{SNR}^+_{\mathrm{g}} = \frac{P^+_{\mathrm{s}}}{P^+_{\mathrm{g}}} = M\frac{P^-_{\mathrm{s}}}{P^-_{\mathrm{g}}} = M\mathrm{SNR}^-_{\mathrm{g}}, \tag{6.4}$$

indicating that the signal to Gaussian noise has been enhanced by a factor M.

In the case of an in-band single-tone interferer, whose essentially bandwidth, the power of the interferer is not reduced by the receiver. However, such an interferer also has a smaller impact on the signal due to spectrum spreading. So, the SNR is enhanced by the same factor M as in the case of a Gaussian noise.

6.4 Experimental Demonstration

The experimental demonstration in this paper will resort to cascaded C-section phasers implemented in stripline technology following the synthesis procedures presented in [3]. The traces of the designed phasers, and their measured S-parameter and group delay responses are plotted in Fig. 6.3. As required, the two phasers were designed so as to provide opposite-slope and mutually compensating linear chirp responses over the frequency range of the signals. The stretching factor of the phasers is $M = (T_0 + s\Delta\omega)/T_0$ =2.38.

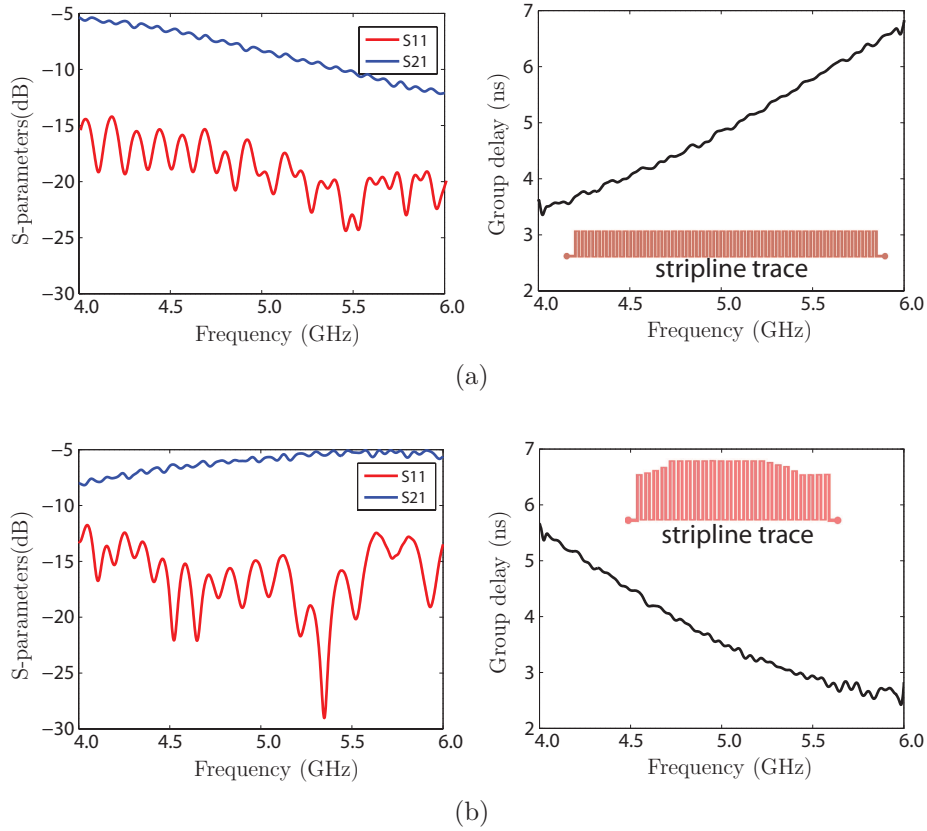

Figure 6.3 Measured responses for the two linear group-delay phasers implemented in cascaded C-section stripline technology for the experimental demonstration [3]. The substrates are Rogers 3602 substrates, with $\epsilon_r = 6.15$ and $\tan\delta = 0.0027$. The insets show the traces of the stripline structures. (a) Up-chirp phaser, slope =+1.602 ns/GHz (= 0.255ns^2/rad). (b) Down-chirp phaser, slope = −1.602 ns/GHz.

The complete experimental transceiver system is shown in Fig. 6.4. For the sake of the proof-of-concept, the noisy channel is emulated by a power combiner that injects into the receiver the sum of the signal produced by the transmitter and of the noise. The input test

signal, $g(t)$ [see Fig. 6.1(a)] is a quasi-Gaussian pulse, of duration $T_0 = 1.5$ ns and bandwidth Δf =1.3 GHz, produced by the pulse-shaper from a rectangular input data pulse. The upconverter modulates the Gaussian pulse at 5 GHz, producing $v_{\rm Tx}^-(t)$. The phaser up-chirps this signal into $v_{\rm Tx}^+(t)$. Hence, given $\Delta\omega = 2\pi \times 1.3$ =8.16 rad/ns and $s = 0.255$ ns^2/rad, the total duration of $v_{\rm Tx}^+(t)$ is $T = T_0 + \Delta T = 3.6$ ns ($\Delta T = s\Delta\omega = 2.1$ ns). Finally, this signal is boosted by an amplifier and its magnitude [see Fig. 6.3(a)] is equalized [28] to avoid signal distortion [1]. The resulted transmit signal is then passed through the channel emulator (power combiner with noise addition). The receiver essentially consists in the down-chirp phaser, which transforms the received noisy signal $v_{\rm Rx}^-(t) + v_n(t)$ into the demodulated signal $v_{\rm Rx}^+(t)$, that is visualized on a real-time oscilloscope.

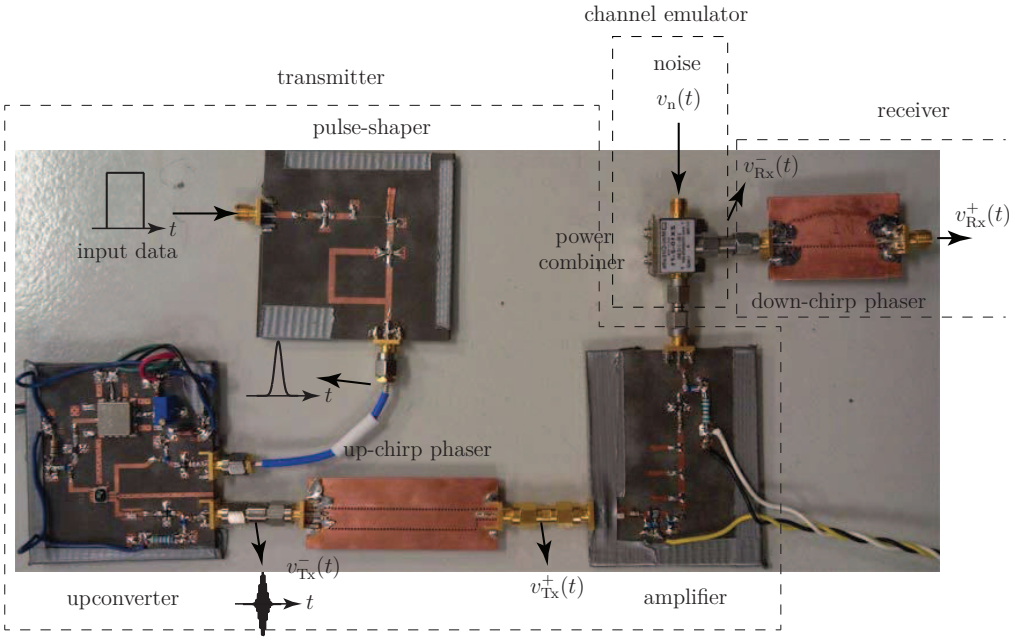

Figure 6.4 Experimental transceiver system using the phasers in Fig. 6.3. The dimensions of the up-chirp and down-chirp phasers are 6.5x2.5 cm and 4x3 cm, respectively.

Figure 6.5 shows the measured results for the received signal in the presence of burst noise. The burst noise magnitude is set such that its peak level equals that of the signal are equal at the input of the receiver (SNR$_b^-$ =0 dB), as shown in Fig. 6.5(a). The signal to burst noise ratio at the output of the down-chirp phaser has been enhanced by 7 dB, as shown in Fig. 6.5(b). The theoretical result for the SNR enhancement in (6.2) is found to be M^2 =5.66 (=7.52 dB), which is in close agreement with the measured SNR enhancement. The measured results for the received signal to Gaussian noise is shown in Fig. 6.6. Here, the signal to Gaussian noise ratio is set to SNR$_g^- = \frac{P_{s,avg}^-}{P_{g,avg}^-}$ =1.3 dB, where $P_{s,avg}^-$ and $P_{g,avg}^-$ are the average signal power and average noise power, respectively. As shown in Fig. 6.6(b), the signal to Gaussian noise

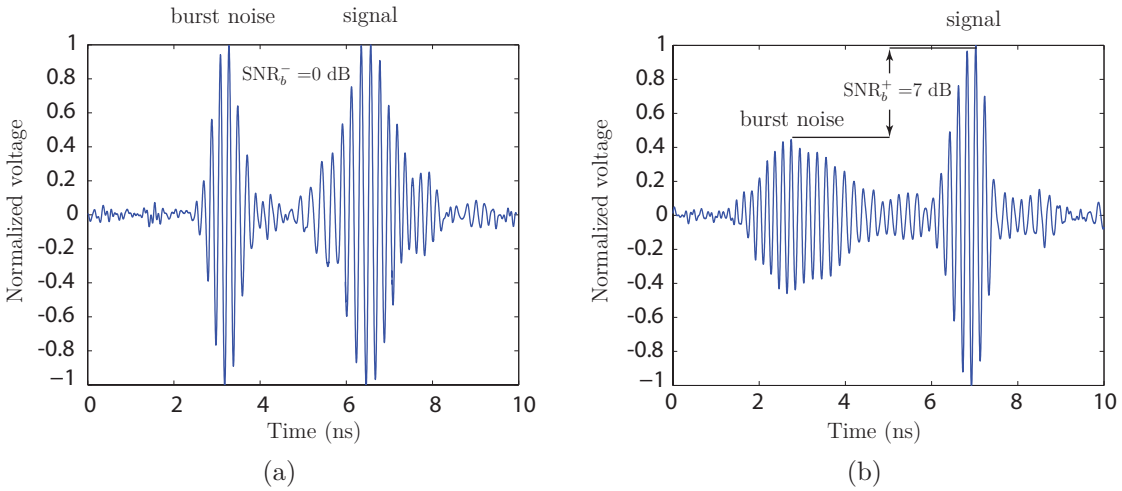

Figure 6.5 Experimental results of the received signal in presence of the burst noise. (a) Before the down-chirp phaser, $v_{\mathrm{Rx}}^{-}(t)$, representing SNR_b^- =0 dB. (b) After the down-chirp phaser, $v_{\mathrm{Rx}}^{+}(t)$, representing SNR_b^+ =7 dB.

ratio at the output of the down-chirp phaser is enhanced by 4.1 dB. This is again in close agreement with the theoretical prediction of (6.4), M =2.38 (=3.76 dB).

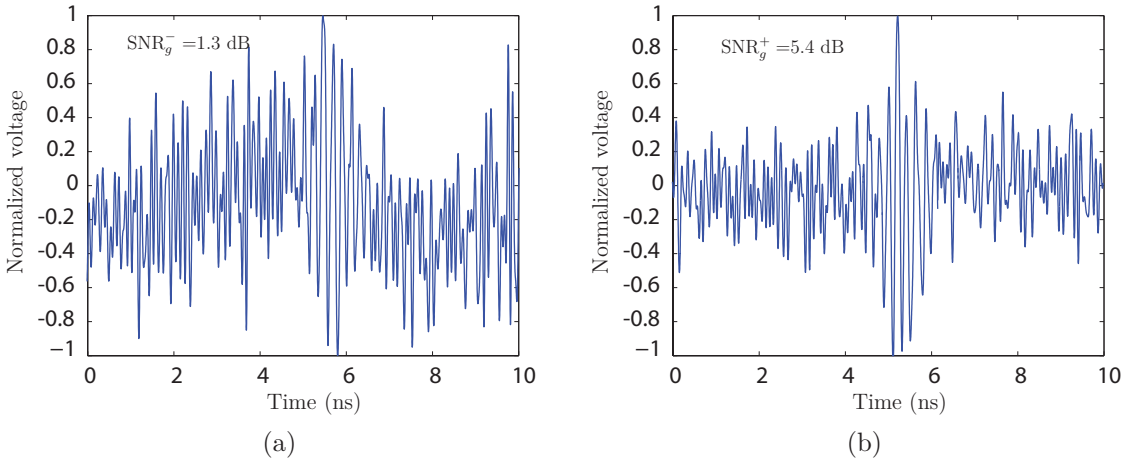

Figure 6.6 Experimental results of the received signal in presence of the Gaussian noise. (a) Before the down-chirp phaser, $v_{\mathrm{Rx}}^{-}(t)$, representing SNR_g^- =1.3 dB. (b) After the down-chirp phaser, $v_{\mathrm{Rx}}^{+}(t)$, representing SNR_g^+ =5.4 dB.

6.5 Conclusions

We have proposed and experimentally demonstrated the concept of SNR enhancement in impulse radio transceivers using phasers of opposite chirping slopes. It has been shown that SNR enhancement by factors M^2 and M are achieved for burst noise and Gaussian noise, respectively, where M is the stretching factor of the phasers. The transceiver system is simple, low-cost and frequency scalable, and may therefore be suitable for broadband impulse radio ranging and communication applications. Its limitations are related to those of the phaser. The bandwidth of the input signal should not exceed its bandwidth. Moreover, the power of the burst noise should not exceed $M^2 P_s^-$, while that of the Gaussian noise should not exceed $M P_s^-$ for detection to be possible.

CHAPTER 7 GENERAL DISCUSSION

Table 7.1 shows a list of various analog signal processing applications classified into three different categories in the wireless and radio technology. Some of these applications have been presented in this thesis.

Table 7.1 R-ASP application classification

Radiocommunication	Sensing and Detection	General Purpose
Impulse Radio	Frequency Sniffer	Signal Compressor
FDM Receiver	Frequency Sector Detector	Non-Linear Phase Shifter
	RFID	Distortion Equalizer

As an R-ASP application in the category of radiocommunication, a real time frequency division multiplexing (FDM) receiver based on a C-section phaser in the impulse regime, has been proposed [16]. Considering that an FDM signal is a multi-tone signal, a phaser can discriminate its frequency components of the FDM signal in time, using its frequency discrimination characteristics. Thus, this receiver demultiplexes the FDM signal in the time domain by mapping each of its frequency components to its corresponding group delay. Compared to conventional FDM receivers, which utilize several analog and digital components for demultiplexing, making the receiver architecture complex, the proposed FDM receiver employs a single phaser in a simpler architecture.

The proposed frequency sniffer in Chapter 5, detects the presence or absence of active frequency channels in its environment, using an omnidirectional antenna. However this system can not detect the direction of the arrival frequencies. A real-time sector detection has been proposed as a part of this PhD work based on a reconfigurable CRLH leaky-wave antenna to detect the frequencies and their direction of arrivals [66].

RFID is another application of the ASP which is proposed in the sensing and detection category [67]. This application uses a phaser as a tag. The RFID reader generates a sequence pulses, modulated in different frequencies as an interrogating signal. The RFID tag receives this interrogating signal and assigns it a PPM code in the form of a sequence of time-delayed pulses based on the phaser frequency group-delay response. The proposed concept offers system simplicity, frequency scalability, and M-ary coding capability for large ID coding diversity.

Finally, the application of the R-ASP can be also found in the beamforming array antenna

applications as well. In this case an arbitrary phaser can be used as frequency dependent phase shifter which steers the radiation beam in a given direction according to the phaser dispersion characteristics.

7.1 R-ASP Limitations and Constraints

R-ASP system has a good response at high frequency compared to the DSP system which works very well at low frequency. However, R-ASP system has some constraints, which are needed to be improved for high frequency and high bandwidth application. The resolution enhancement of the R-ASP, which is obtained by group-delay enhancement of the phaser, increases the size and insertion loss of the R-ASP system, and consequently, decreases the efficiency of the system. Also, Phaser design and fabrication for higher order group-delay frequency response applications, such as DCMA [6] and frequency sniffer is difficult. So, the phaser technology and synthesis need to be improved to get arbitrary responses at high frequency.

CHAPTER 8 CONCLUSIONS AND FUTURE WORKS

This thesis proposes novel techniques related to R-ASP systems, R-ASP enhancement techniques, and applications which has a great potential for radiocommunication, radar, sensor, and instrumentation. Phaser has been employed as the core component in the proposed R-ASP systems.

Chapter 2 introduced the fundamentals of phaser, which is the core component of an R-ASP system ; it reviews phaser technologies, explains the characteristics of the microwave phasers, discusses system problematics and proposes enhancement techniques for higher R-ASP performance.

Chapter 3 presents the article entitled "Increased Group Delay Slope Loop System for Enhanced-Resolution Analog Signal Processing". In this article, a novel feedback loop technique has been proposed to increase the time-frequency resolution of the phaser for microwave analog signal processing systems. This technique has been experimentally demonstrated in a frequency meter and a frequency discriminator. The feedback loop technique is a solution for the group-delay frequency enhancement of the phaser, rather than cascading phasers with a higher insertion loss and a bigger size which leads the system to a sever SNR reduction.

Chapter 4 is the article "Low-Cost Analog Pulse Compression Technique based on Mixing with an Auxiliary Pulse". The complexity of the UWB pulse generation, which is used in R-ASP applications has been addressed, and a simple technique based on mixing with an auxiliary pulse has been proposed and experimentally demonstrated in this article. Due to its analog nature, the proposed system is frequency scalable, low power consumption, easy to implement, and flexible.

Chapter 5 discusses a "Distortion-less Real-Time Spectrum Sniffing Based on a Stepped Group-Delay Phaser ". In this proposed system, the pulse spreading problem of the conventional linear group delay phaser for frequency sniffing application has been discussed, and the new stepped group delay phaser in order to suppress the frequency resolution limitation has been proposed. The proposed real-time spectrum sniffer is simple, low-cost with straightforward frequency scalability.

Chapter 6 presents an "Enhanced-SNR Impulse Radio Transceiver based on Phasers". In this system, the SNR enhancement of the impulse radio based on the up and down chirp phasers with a stretching factor, M is achieved for burst noise and gaussian noise. It has been shown that SNR enhancement by factors M^2 and M are achieved for burst noise and Gaussian noise,

respectively. The transceiver system is simple, low-cost and frequency scalable, and may therefore be suitable for broadband impulse radio ranging and communication applications. Its limitations are related to those of the phaser. Some possible extensions and the future works for ASP in radio application are explained as below.

Frequency Division Multiple Access (FDMA)

As an R-ASP application, a real-time FDM receiver has been proposed in the article [16] based on a phaser. The proposed receiver is able to demodulate the FDM signal by simply mapping each frequency component to its corresponding group delay, and hence separating the time domain signals for detection. The proposed receiver only requires a single component for demodulation, thus simplifying the receiver architecture compared to conventional FDM receivers. Furthermore, as a future work, a real-time frequency division multiple access (FDMA) system may be achieved by using multiple parallel phasers.

Phaser as a Non-Linear Phase Shifter

Phasers can be used in beamforming array antennas. Using an arbitrary phaser as a non-linear arbitrary phase shifter, the angle of the antenna main beam can be steered. In particular, scanning sensitivity with frequency can be controlled by using phasers with different group delay responses. Furthermore, It may also provide solutions for solving beam squinting problems in antenna arrays.

Dispersion Code Multiple Access (DCMA)

Phasers also have promising applications in chirp spread spectrum (CSS) encoding [68]. CSS technique uses wide-band linear chirp signal to encode digital data, thereby making it robust to channel noise. However, this technique has currently not been used for multiple access application. The new phaser techniques with arbitrary linear and non-linear group delays, can be used as chirp encoders in the transmitters which can only be decoded by the complimentary phasers with an inverse delay response of the transmitting phasers, Fig. 8.1. This technique has been patented is currently investigated [6].

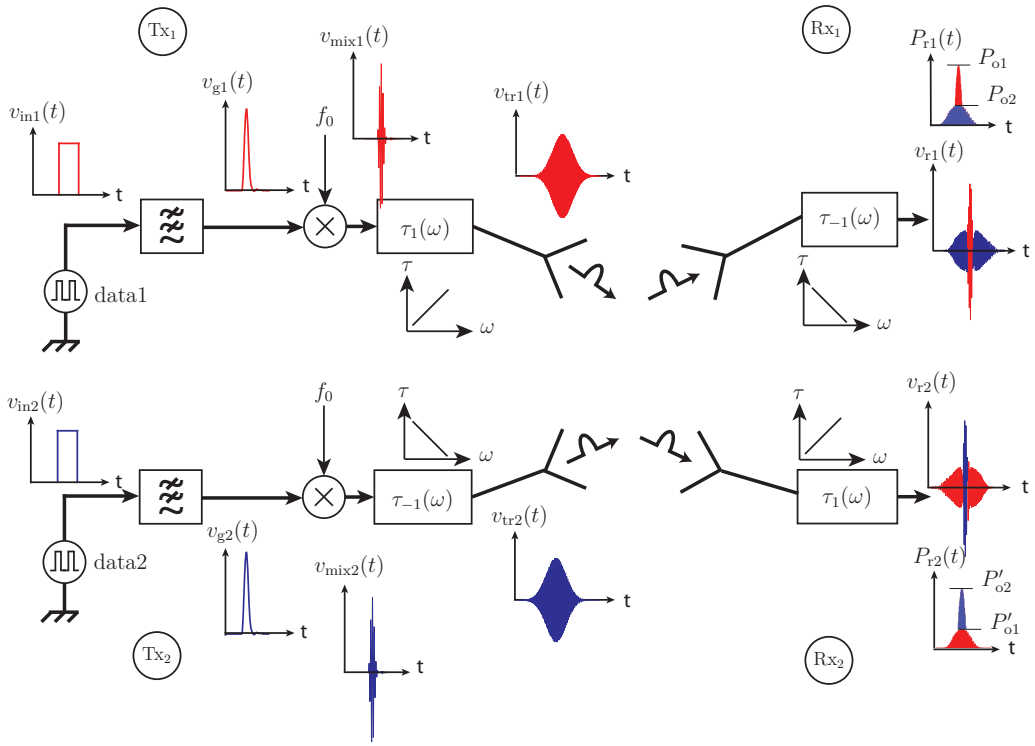

Figure 8.1 Principle of the proposed DCMA system.

REFERENCES

[1] C. Caloz, S. Gupta, Q. Zhang, and B. Nikfal, "Analog signal processing: A possible alternative or complement to dominantly digital radio schemes," *IEEE Microwave Magazine*, vol. 14, no. 6, pp. 87–103, Sep.-Oct. 2013.

[2] B. Nikfal, S. Gupta, and C. Caloz, "Increased group delay slope loop system for enhanced-resolution analog signal processing," *IEEE Trans. Microwave Theory Tech.*, vol. 59, no. 6, pp. 1622 – 1628, Jun. 2011.

[3] S. Gupta, A. Parsa, E. Perret, R. V. Snyder, R. J. Wenzel, and C. Caloz, "Group delay engineered non-commensurate transmission line all- pass network for analog signal processing," *IEEE Trans. Microwave Theory Tech.*, vol. 58, no. 9, pp. 2392–2407, Sep. 2010.

[4] S. Gupta, S. Abielmona, and C. Caloz, "Microwave analog real-time spectrum analyzer (RTSA) based on the spectral spatial decomposition property of leaky-wave structures," *IEEE Trans. Microw. Theory Tech.*, vol. 57, no. 12, pp. 2989–2999, Dec. 2009.

[5] B. Nikfal, D. Badiere, M. Repeta, B. Deforge, S. Gupta, and C. Caloz, "Distortionless real-time spectrum sniffing based on a stepped group-delay phaser," *IEEE Microw. Wireless Compon. Lett.*, vol. 22, no. 11, pp. 601–603, Nov. 2012.

[6] B. Nikfal, C. caloz, and M. Salem, "A method and apparatus for encoding data using instantaneous frequency dispersion," *US patent 62/002,978*, May 2014.

[7] B. Xiang, A. Kopa, F. Zhongtao, and A. B. Apsel, "Theoretical analysis and practical considerations for the integrated time-stretching system using dispersive delay line (DDL)," *IEEE Trans. Microw. Theory Tech.*, vol. 60, no. 11, pp. 3449–3457, Nov. 2012.

[8] M. A. Muriel, J. A. na, and A. Carballar, "Real-time fourier transformer based on fiber gratings," *Opt. Lett.*, vol. 24, no. 1, pp. 1–3, Jan. 1999.

[9] S. Abielmona, S. Gupta, and C. Caloz, "Experimental demonstration and characterization of a tunable CRLH delay line system for impulse/continuous wave," *IEEE Antennas Wireless Propag. Lett.*, vol. 17, no. 12, pp. 864–866, Dec. 2007.

[10] H. V. Nguyen and C. Caloz, "Composite right/left-handed delay line pulse position modulation transmitter," *IEEE Microwave Wireless Compon. Lett.*, vol. 18, no. 5, pp. 527–529, Aug. 2008.

[11] S. Abielmona, S. Gupta, and C. Caloz, "Compressive receiver using a CRLH-based dispersive delay line for analog signal processing," *Microwave Theory and Techniques, IEEE Transactions on*, vol. 57, no. 11, pp. 2617–2626, 2009.

[12] A. M. Kawalec, "SAW dispersive delay lines in radar signal processing," *IEEE International Radar Conference*, pp. 732 – 736, May. 1995.

[13] S. Gupta and C. Caloz, "Analog real-time fourier transformer using a group delay engineered c-section all-pass network," *EEE International Symposium on Antennas and Propagation and CNC/USNC/URSI National Radio Science Meeting*, July 2010.

[14] B. Nikfal, Q. Zhang, and C. Caloz, "Enhanced-SNR impulse radio transceiver based on phasers," *IEEE Microw. Wireless Compon. Lett.*, vol. 24, no. 11, pp. 778–780, Nov. 2014.

[15] M. A. G. Laso, T. Lopetegi, M. J. Erro, D. Benito, M. J. Garde, M. A. Muriel, M. Sorolla, and M. Guglielmi, "Composite right/left-handed delay line pulse position modulation transmitter," *IEEE Trans. Microwave Theory and Techniques*, vol. 51, no. 3, pp. 705–717, March 2003.

[16] B. Nikfal and C. Caloz, "Low-complexity and frequency-scalable analog real-time FDM receiver based on a dispersive delay structure," *The 41st European Microwave Conference, Manchester, England*, pp. 397–400, Oct. 2011.

[17] Q. Zhang, D. L. Sounas, and C. Caloz, "Synthesis of cross-coupled reduced-order dispersive delay structures (DDS) with arbitrary group delay and controlled magnitude," *IEEE Trans. Microwave Theory Tech.*, vol. 61, no. 3, pp. 1043–1052, Mar. 2013.

[18] W. S. Ishak, "Magnetostatic wave technology: A review," *Proc. of the IEEE*, vol. 76, no. 2, pp. 171–187, Feb. 1998.

[19] C. K. Campbell, "Surface acoustic wave devices for mobile and wireless communications," *Academic Press, 1st Ed.*, 1998.

[20] S. Gupta, D. L. Sounas, H. V. Nguyen, Q. Zhang, and C. Caloz, "CRLH-CRLH C-section dispersive delay structures with enhanced group delay swing for higher analog signal processing resolution," *IEEE Trans. Microw. Theory Tech.*, vol. 60, no. 21, pp. 3939–3949, Dec. 2012.

[21] M. N. Laboratory, "Development of fabrication techniques for building integrated-optical grating-based filters." [Online]. Available: http://nanoweb.mit.edu/annual-report00/16.

[22] J. D. Schwartz, J. Azaña, and D. Plant, "Experimental demonstration of real-time spectrum analysis using dispersive microstrip," *IEEE Microw. Wireless Compon. Lett.*, vol. 16, no. 4, pp. 215–217, Apr. 2006.

[23] Q. Zhang, S. Gupta, and C. Caloz, "Synthesis of narrow-band rejection-type phaser with arbitrary prescribed group delay," *IEEE Trans. Microw. Theory Tech.*, vol. 60, no. 8, pp. 2394–2402, Aug. 2012.

[24] J. D. Adam, M. R. Daniel, P. R. Emtage, and S. H. Talisa, "Magnetostatic waves," in *Thin Films for Advanced Electronic Devices: Volume 15*, M. H. Francombe and J. L. Vossen, Eds. Academic Press, 1991.

[25] O. Tigli and M. E. Zaghloul, "Finite element moelin and analysis of surface acoustic wave devices in CMOS technology," *IEEE Trans. Compon. Packag. Manuf. Technol.*, vol. 2, no. 6, pp. 1021–1029, Jun. 2012.

[26] C. Caloz and T. Itoh, *Electromagnetic Metamaterials, Transmission Line Theory and Microwave Applications*. Wiley - IEEE Press, 2006.

[27] Q. Zhang, J. W. Bandler, and C. Caloz, "Design of dispersive delay structures (DDSs) formed by coupled c-sections using predistortion with space mapping," *IEEE Trans. Microw. Theory Tech.*, vol. 61, no. 12, pp. 4040–4051, Nov. 2013.

[28] S. Gupta, B. Nikfal, and C. Caloz, "Amplitude equalized transmission line dispersive delay structure for analog signal processing," *Int. Conference on Telecommunications in Modern Satellite,Cable and Broadcasting Services (TELSIKS), Nis, Serbia*, pp. 379–382, Oct. 2011.

[29] Q. Zhang, S. Gupta, and C. Caloz, "Synthesis of narrowband reflection-type phasers with arbitrary prescribed group delay," *IEEE Journals Magazines*, vol. 60, no. 8, pp. 2394–2404, June 2012.

[30] W. Hendrik, "Network analysis and feedback amplifier design," *D. Van Nostrandf, reprint ed.*, 1951.

[31] J. D. Jackson, "Classical electrodynamics," *Wiley, 3rd Ed.*, 1998.

[32] G. P. Agarwal, "Nonlinear fiber optics," *Academic Press*, 2005.

[33] W. D. White, "Signal translation apparatus utilizing dispersive network and the like, for panoramix reception, amplitude-controlling frequency response, signal frequency gating, frequency-time conversion, etc." *U.S. Patent 2954465*, Sep. 1960.

[34] M. Lewis, "Saw and optical signal processing," *Proc. of the IEEE Ultrasonics Symp., Rotterdam, Netherlands*, pp. 800–809, Sep. 2005.

[35] M. l Skolnik, "Introduction to radar systems," *McGraw-Hill, 3rd Ed.*, 2001.

[36] D. D. Stancil, "Theory of magnetostatic waves," *Springer-Verlag Berlin and Heidelberg GmbH & Co. K*, 1993.

[37] C. K. Campbell, "Passive microwave device applications of high-temperature superconductors," *Cambridge University Press, 1st Ed.*, 2006.

[38] J. D. Schwartz, J. Azana, and D. V. Plant, "Experimental demonstration of real-time spectrum analysis using dispersive microstrip," *IEEE Microwave and Wireless Components Lett.*, vol. 16, no. 4, pp. 215–218, April 2006.

[39] S. Gupta and C. Caloz, "Analog signal processing in transmission line metamaterial structures," *Radioengineering*, vol. 18, no. 2, pp. 155–167, June 2009.

[40] C. Caloz, "Metamaterial dispersion engineering concepts and applications," *Proc. IEEE*, vol. 99, no. 10, pp. 1711–1719, Oct. 2011.

[41] J. J. Snyder, "An ultra-high resolution frequency meter," *Thirty Fifth Annual Frequency Control Symposium 1881*, pp. 464–469, 1981.

[42] L. V. D. Steen, "A low frequency meter with instantaneous response," *IEEE Transactions on Biomedical Engineering*, vol. BME-26, no. 3, pp. 137–140, March 1979.

[43] J. L. Stewart, "A general theory for frequency discriminators containing null networks," *Proceedings of the IRE*, vol. 40, no. 1, pp. 55–57, Jan. 1952.

[44] H. G. Cho and C. W. W. Lee, "Microwave transmission line frequency discriminators," *Microwave Symposium Digest, 1986 IEEE MTT-S International*, pp. 279–282, June 1986.

[45] S. S. Haykin, "Active network theory," *Addison-Wesley*, 1970.

[46] G. L. Matthaei, L. Young, and E. M. T. Jones, "Microwave filters, impedance matching networks and coupling structures," *McGraw Hill*, 1965.

[47] H. S. Hewitt, "A computer designed, 720 to 1 microwave compression filter," *IEEE Trans. Microwave Theory and Techniques*, vol. 15, no. 12, pp. 687–694, Dec. 1967.

[48] A. S. Sedra, "Microelectronic circuits (oxford series in electrical engineering)," *Oxford University Press ; 4 edition*, June 1997.

[49] S. Azevedo and T. E. McEwan, "Micropower impulse radar," *IEEE Potentials*, vol. 16, no. 2, pp. 15–20, Apr/May 1997.

[50] H. M. Jafari, W. Liu, S. Hranilovic, and M. J. Deen, "Ultrawideband radar imaging system for biomedical applications," *Journal of Vacuum Science & Technology A: Vacuum, Surfaces, and Films*, vol. 24, no. 3, pp. 752–757, May 2006.

[51] P. Tortoli, F. Guidi, and C. Atzeni, "Digital vs. SAW matched filter implementation for radar pulse compression," *Proceedings of IEEE Ultrasonics Symposium*, vol. 1, pp. 199–202, Nov. 1994.

[52] Y. Zheng, Z. He, and Z. Zong, "Design of the high-powered digital pulse compression real-time processing system based on ADSP-TS203," *International Conference on Radar CIE '06*, pp. 1–4, Oct. 2006.

[53] R. Withers, A. Anderson, P. Wright, and S. Reible, "Superconductive tapped delay lines for microwave analog signal processing," *IEEE Transactions on Magnetics*, vol. 19, no. 3, pp. 480 – 484, May. 1983.

[54] C. Wang and J. P. Yao, "Chirped microwave pulse compression using a photonic microwave filter with a nonlinear phase response," *IEEE Trans. Microwave Theory Tech.*, vol. 57, no. 2, pp. 496–504, Jan. 2009.

[55] J. Lee, J. D. Cressler, and A. J. Joseph, "A 5-6 GHz SiGe HBT monolithic active isolator for improving reverse isolation in wireless systems," *IEEE Microw. Wireless Compon. Lett.*, vol. 15, no. 4, pp. 220–222, Apr. 2005.

[56] C. Coleman, "Oscillators and phase locked loops," *Chapter 5, 1st Ed., Cambridge University Press, New York*, pp. 108–120, 2004.

[57] F. Harris, "A coupled multichannel filter bank and sniffer spectrum analyzer," *Cognitive Radio Oriented Wireless Networks and Communications (CROWNCOM)*, pp. 1–5, Jun. 2010.

[58] L. Berlemann and S. Mangold, "Cognitive radio for dynamic spectrum access," *Chapter 1-4, John Wiley, 1st Ed.*, pp. 1–70, 2009.

[59] M. Hunter, A. Kourtellis, C. Ziomek, and W. Mikhael, "Fundamentals of modern spectral analysis," *AUTOTESTCON*, pp. 1–5, Sep. 2010.

[60] H. V. Nguyen and C. Caloz, "Composite right/left-handed delay line pulse position modulation transmitter," *IEEE Microw. Wireless Compon. Lett.*, vol. 18, no. 8, pp. 527–529, Aug. 2008.

[61] W. G. Alliance, "Wigig white paper: defining the future of multi-gigabit wireless communications," *Tech. Rep. Wireless Gigabit Alliance, Beaverton, Ore, USA*, 2009.

[62] H. Hedayati and K. Entesari, "A 90-nm CMOS UWB impulse radio transmitter with 30-db in-band notch at ieee 802.11a system," *IEEE Trans. Microw. Theory Tech.*, vol. 61, no. 12, pp. 4220–4232, Dec. 2013.

[63] A. Medi and W. Namgoong, "A high data-rate energy-efficient interference-tolerant fully integrated CMOS frequency channelized UWB transceiver for impulse radio," *IEEE Journal of Solid-State Circuits*, vol. 43, no. 4, pp. 974–980, April 2008.

[64] T. Terada, S. Yoshizumi, M. Muqsith, Y. Sanada, and T. Kuroda, "A CMOS ultra-wideband impulse radio transceiver for 1-mb/s data communications and 2.5-cm range finding," *IEEE Journal of Solid-State Circuits*, vol. 41, no. 4, pp. 891–898, April 2006.

[65] Q. Zhang, D. L. Sounas, S. Gupta, and C. Caloz, "Wave interference explanation of group delay dispersion in resonators," *IEEE Antenna and Propagation Magazine*, vol. 55, no. 2, pp. 212–227, May 2013.

[66] B. Nikfal and C. Caloz, "Real-time sector detection based on a reconfigurable leaky-wave antenna," *European Conf. Antennas Propag. (EuCAP), Gothenburg, Sweden*, pp. 1729–1731, Apr. 2013.

[67] S. Gupta, B. Nikfal, and C. Caloz, "Chipless RFID system based on group delay engineered dispersive delay structures," *IEEE Microw. Wireless Compon. Lett.*, vol. 10, pp. 1366–1368, Dec. 2011.

[68] "IEEE computer society," *IEEE Standard 802.15.4a-2007 New York, NY: IEEE*, Aug. 2007.

APPENDIX A LIST OF PUBLICATIONS

Journal Papers and Letters

1. B. Nikfal, Q. Zhang, and C. Caloz, Enhanced-SNR, impulse radio transceiver based on phasers, *IEEE Microwave Wireless Compon. Lett*, Vol. 24, no. 11, pp. 778-780, Nov. 2014.
2. C. Caloz, S. Gupta, Q. Zhang, and B. Nikfal, Analog signal processing, *IEEE Microwave Mag.*, vol. 14, no. 6, pp. 87-103, May. 2013.
3. B. Nikfal, Q. Zhang, and C. Caloz, Comment on theoretical analysis and practical considerations for the integrated time-stretching system using dispersive delay line (DDL), *IEEE Trans. Microwave Theory Tech.*, vol. 61,Issue. 5, pp. 1973, May. 2013.
4. B. Nikfal, D. Badiere, M. Repeta, B. Deforge, S. Gupta, and C. Caloz, Distortionless real-time spectrum sniffing based on a stepped group-delay phaser, *IEEE Microw. Wireless Compon. Lett.*, Vol. 22,no. 11, pp. 601-603, Nov. 2012.
5. B. Nikfal, S. Gupta, and C. Caloz, Low-cost and efficient pulse compression based on mixing with an auxiliary pulse, *IEEE Microw. Wireless Compon. Lett.*, vol. 22, no. 3, pp. 150-152, Mar. 2012.
6. Y. Horii, S. Gupta, B. Nikfal, and C. Caloz, Multilayer broadside-coupled dispersive delay structures for analog signal processing, *IEEE Microw. Wireless Compon. Lett.*, vol. 22, no. 1, pp. 1-3, Jan. 2012.
7. S. Gupta, B. Nikfal, and C. Caloz, Chipless RFID system based on group delay engineered dispersive delay structures, *IEEE Antennas Wirel. Propag. Lett.*, vol. 10, pp. 1366-1368, Dec. 2011.
8. B. Nikfal, S. Gupta, and C. Caloz, Increased group delay slope loop system for enhanced-resolution analog signal processing, *IEEE Trans. Microw. Theory Tech.*, vol. 59, no. 6 pp. 1622-1628, Jun. 2011.

Conference Publications

1. Q. Zhang, B. Nikfal, and C. Caloz. High-resolution real-time spectrum sniffer for wireless communication, *in URSI Int. Symp. on Electromagnetic Theory (EMTS)*, Spokane, Washington, pp. 64-66, May. 2013.

2. B. Nikfal, and C. Caloz. Real-time sector detection based on a reconfigurable leaky-wave antenna, *in European Conf. Antennas Propag. (EuCAP)*, Gothenburg, Sweden, pp. 1729-1731, Apr. 2013.
3. C. Caloz, S. Gupta, B. Nikfal, and Q. Zhang. Analog signal processing (ASP) for high-speed microwave and millimeter-wave systems, *in IEEE Asia Pacific Microw. Conf. (APMC)*, Kaohsiung, Taiwan, pp. 691-692, Dec. 2012.
4. B. Nikfal and C. Caloz. Hybrid time-frequency RFID system, *in IEEE MTT-S Int. Microw. Symp. (IMS)*, Montreal, Canada, Jun. 2012.
5. B. Nikfal and C. Caloz. Low-complexity and frequency-scalable analog real-time FDM receiver based on a dispersive delay structure, *in IEEE European Microw. Conf. (EuMC)*, Manchester, England, pp. 397-400, Oct. 2011.
6. S. Gupta, B. Nikfal, and C. Caloz. Amplitude equalized transmission line dispersive delay structure for analog signal processing, *in Int. Conference on Telecommunications in Modern Satellite, Cable and Broadcasting Services (TELSIKS)*, Nis, Serbia, pp. 379-382, Oct 2011.
7. T. Kaneko, Y. Horii, S. Gupta, B. Nikfal, and C. Caloz. Design of multilayer broadside-coupled dispersive delay structures (DDS) for real-time analog signal processing, *in IEICE Society Conf.*, Sapporo, Japan, pp. 86, Sep. 2011.
8. S. Gupta, B. Nikfal and C. Caloz. RFID System based on Pulse-Position Modulation using Group Delay Engineered Microwave C-Sections, *Asia Pacific Microwave Conference 2010*, Yokohama, Japan, pp. 203-206, Dec. 2010.

Patents

1. Nikfal Babak, Caloz Christophe, and Salem Mohamed, “A method and apparatus for encoding data using instantaneous frequency dispersion," US 62/002,978, May 2014